Research Article | Vol. 24, No. 21 | 17 Oct 2016 | OPTICS EXPRESS 24665
Optics EXPRESS

Aberration fields of off-axis two-mirror astronomical telescopes induced by lateral misalignments

GUOHAO JU,[1,2,*] CHANGXIANG YAN,[1] ZHIYUAN GU,[1] AND HONGCAI MA[1]

[1]*Changchun Institute of Optics, Fine Mechanics and Physics, Chinese Academy of Sciences, Changchun 130033, China*
[2]*University of Chinese Academy of Sciences, Beijing 100049, China*
[*]*juguohao123@163.com*

Abstract: This paper presents a systematic and in-depth discussion for the aberration fields of off-axis two-mirror astronomical telescopes with an offset pupil that is induced by lateral misalignment. Based on the framework of nodal aberration theory and a system level pupil coordinate transformation, the aberration function for misaligned off-axis telescopes is derived. Some general descriptions for the misalignment-induced aberrations are presented. The specific astigmatic and coma aberration field characteristics in off-axis two-mirror telescopes are then discussed. The precision of the presented aberration expressions is demonstrated. The discrepancies between the ray tracing data and aberration expressions are explicated. Then the inherent relationships between the astigmatism and coma aberration fields are revealed and explicated. Based on this knowledge, some quantitative discussions are further presented for determining the misalignments used to compensate for the effects of primary mirror astigmatic figure errors as well as separating these two effects when coupled. Other effects of lateral misalignments are also presented, especially the field-constant focal shift, which is only sensitive to the lateral misalignments in the symmetry plane of the nominal off-axis system. A quantitative discussion is also presented which explains the reason why trefoil aberration in off-axis telescopes is more sensitive to lateral misalignments. Most of the results presented in this paper can be extended to the other off-axis astronomical telescopes with more freedoms.

OCIS codes: (080.0080) Geometric optics; (080.1010) Aberrations (global); (110.6770) Telescopes; (220.1140) Alignment; (220.1080) Active or adaptive optics.

References and links

1. J. R. Kuhn and S. L. Hawley, "Some astronomical performance advantages of off-axis telescopes," Publ. Astron. Soc. Pac. **111**(759), 601–620 (1999).
2. M. Bartelmann and P. Schneider, "Weak gravitational lensing," Phys. Rep. **340**(4–5), 291–472 (2001).
3. F. Zeng, X. Zhang, J. Zhang, G. Shi, and H. Wu, "Optics ellipticity performance of an unobscured off-axis space telescope," Opt. Express **22**(21), 25277–25285 (2014).
4. W. Cao and N. Gorceix, *et al*., "First Light of the 1.6 meter off-axis New Solar Telescope at Big Bear Solar Observatory," Proc. SPIE **7333**, 73330 (2010).
5. G. Moretto and J. R. Kuhn, "Optical performance of the 6.5-m off-axis New Planetary Telescope," Appl. Opt. **39**(16), 2782–2789 (2000).
6. M. A. Lundgren and W. L. Wolfe, "Alignment of a three-mirror off-axis telescope by reverse optimization," Opt. Eng. **30**(3), 307–311 (1991).
7. H. Lee, G. B. Dalton, I. A. J. Tosh, and S.-W. Kim, "Computer-guided alignment II :Optical system alignment using differential wavefront sampling," Opt. Express **15**(23), 15424–15437 (2007).
8. R. Upton and T. Rimmele, "Active reconstruction and alignment strategies for the Advanced Technology Solar Telescope," Proc. SPIE **7793**, 77930E (2010).
9. R. V. Shack and K. P. Thompson, "Influence of alignment errors of a telescope system," Proc. SPIE **251**, 146–153 (1980).
10. K. P. Thompson, "Aberration fields in tilted and decentered optical systems," Ph.D. dissertation (University of Arizona, Tucson, Arizona, 1980).
11. K. Thompson, "Description of the 3rd-order optical aberrations of near-circular pupil optical systems without symmetry," J. Opt. Soc. Am. A **22**(7), 1389–1401 (2005).

#268694 http://dx.doi.org/10.1364/OE.24.024665
Journal © 2016 Received 17 Jun 2016; revised 22 Aug 2016; accepted 22 Aug 2016; published 14 Oct 2016

Optics EXPRESS

12. K. P. Thompson, "Multinodal 5th-order optical aberrations of optical systems without rotational symmetry: spherical aberration," J. Opt. Soc. Am. A **26**(5), 1090–1100 (2009).
13. K. P. Thompson, "Multinodal 5th-order optical aberrations of optical systems without rotational symmetry: the comatic aberrations," J. Opt. Soc. Am. A **27**(6), 1490–1504 (2010).
14. K. P. Thompson, "Multinodal 5th-order optical aberrations of optical systems without rotational symmetry: the astigmatic aberrations," J. Opt. Soc. Am. A **28**(5), 821–836 (2011).
15. H. H. Hopkins, *The Wave Theory of Aberrations* (Oxford on Clarendon Press, 1950).
16. R. A. Buchroeder, "Tilted component optical systems," Ph.D. dissertation (University of Arizona, Tucson, Arizona, 1976).
17. T. Schmid, K. P. Thompson, and J. P. Rolland, "Misalignment-induced nodal aberration fields in two-mirror astronomical telescopes," Appl. Opt. **49**(16), D131–D144 (2010).
18. K. P. Thompson, T. Schmid, and J. P. Rolland, "The misalignment induced aberrations of TMA telescopes," Opt. Express **16**(25), 20345–20353 (2008).
19. Z. Gu, C. Yan, and Y. Wang, "Alignment of a three-mirror anastigmatic telescope using nodal aberration theory," Opt. Express **23**(19), 25182–25201 (2015).
20. T. Schmid, J. P. Rolland, A. Rakich, and K. P. Thompson, "Separation of the effects of astigmatic figure error from misalignments using Nodal Aberration Theory (NAT)," Opt. Express **18**(16), 17433–17447 (2010).
21. K. Fuerschbach, J. P. Rolland, and K. P. Thompson, "Extending nodal aberration theory to include mount-induced aberrations with application to freeform surfaces," Opt. Express **20**(18), 20139–20155 (2012).
22. K. Fuerschbach, J. P. Rolland, and K. P. Thompson, "Theory of aberration fields for general optical systems with freeform surfaces," Opt. Express **22**(22), 26585–26606 (2014).
23. G. Ju, C. Yan, Z. Gu, and H. Ma, "Computation of astigmatic and trefoil figure errors and misalignments for two-mirror telescopes using nodal-aberration theory," Appl. Opt. **55**(13), 3373–3386 (2016).
24. E. Hansen, R. Price, and R. Hubbard, "Advanced Technology Solar Telescope Optical Design," Proc. SPIE **6267**, 62673Z (2006).
25. K. P. Thompson, T. Schmid, O. Cakmakci, and J. P. Rolland, "Real-ray-based method for locating individual surface aberration field centers in imaging optical systems without rotational symmetry," J. Opt. Soc. Am. A **26**(6), 1503–1517 (2009).
26. J. Wang, B. Guo, Q. Sun, and Z. Lu, "3rd-order aberration fields of pupil decentered optical systems," Opt. Express **20**(11), 11652–11658 (2012).
27. T. Yang, J. Zhu, W. Hou, and G. Jin, "Design method of freeform off-axis reflective imaging systems with a direct construction process," Opt. Express **22**(8), 9193–9205 (2014).
28. T. Yang, J. Zhu, W. Hou, and G. Jin, "Compact freeform off-axis three-mirror imaging system based on the integration of primary and tertiary mirrors on one single surface," Chin. Opt. Lett. **14**(6), 060801 (2016).

1. Introduction

Off-axis telescopes with unobscured pupil have many advantages over the on-axis, axisymmetric ones, such as lower scattering property, larger emissivity throughput, higher dynamic range, so on [1]. Besides, with the development of astronomy, more and more attention is paid and to the measurement of weak gravitational lensing [2]. Unobscured off-axis telescopes also have simpler and sharper diffraction pattern, meaning not only higher resolution but also some advantages in ellipticity performance, which is of cardinal importance for weak gravitational lensing measurement [3]. However, to date only few large unobstructed off-axis telescopes have been constructed, including New Solar Telescope (NST) [4] and New Planetary Telescope (NPT) [5]. Apart from the fabrication of large off-axis surfaces, another main challenge that hinders the construction of large off-axis telescopes lies in the fine alignment as well as active optical compensation and alignment of this class of telescopes. Some methods have been proposed for the alignment or active alignment of this class of telescopes [6–8]. However, on the one hand, most of them are numerical, which can hardly contribute to an in-depth understanding of effects of misalignments on the net aberration fields in off-axis systems; on the other hand, these methods cannot provide some valuable insights or theoretical guidance for the alignment or active alignment of off-axis systems.

Nodal Aberration Theory (NAT), discovered by Shack [9] and developed by Thompson [10–14] based on the wave aberration theory of Hopkins [15] and the concept of shifted aberration field center attributed to Buchroeder [16], is a powerful tool in studying the aberration behavior of optical systems which contain misaligned, or intentionally tilted and/or decentered components. Schmid et al. [17] utilized NAT to study the misalignment-induced

Optics EXPRESS

nodal aberration fields in two-mirror astronomical telescopes (especially Ritchey Chretien telescopes), and showed that removing field-constant coma simultaneously creates a constraint whereby one of the astigmatic nodes must remain effectively on-axis. This result can explain why the alignment of a large telescope based on axial imagery is insufficient. Thompson et al. [18] used NAT to describe the aberration field dependencies that arise in the presence of misalignments for TMA telescopes, and it is shown that the performance of TMA telescopes is dominated by the field-constant 3rd-order coma which can commonly be seen in two-mirror Ritchey Chretien telescopes, and the field-linear, field-asymmetric, 3rd-order astigmatism which is a new and unique field dependence derived for the first time using NAT. Recently, Gu et al. [19] applied 3rd order and 5th order alignment model based on NAT to the alignment of TMA telescopes, respectively. The result showed that NAT can be utilized to quantitatively calculate the misalignment parameters, and the 5th order alignment model has higher computation accuracy. All these works mentioned above can provide valuable insights and theoretical guidance for the alignment of astronomical telescopes with axisymmetric configurations. However, the aberration field responses of unobstructed off-axis telescopes with offset pupil to misalignments have seldom been discussed in the previous researches. The misalignment-induced aberration fields of off-axis systems are quite different from the on-axis ones. They require further study for better understand.

On the other hand, with the increase in the aperture size of the emerging generation of astronomical telescopes, active optics systems play a more and more important role in maintaining good observation performance, by correcting the aberrations induced by mirror misalignments and surface deformations during observing periods. Nodal aberration theory also contributes a lot to the development of active compensation and alignment strategies for active optics systems. Schmid et al. [20] distinguished the effects of misalignments and primary mirror astigmatic figure error for two-mirror telescopes, based on the characteristic astigmatic nodal properties in the presence of secondary mirror misalignments and primary mirror astigmatic figure error. Fuerschbach et al. [21,22] presented a generalized theoretical formulation for the aberration behavior of non-symmetric optical surfaces and analyzed the impact of three-point mount-induced trefoil deformation on the net aberration fields. It was shown that when an optical surface located away from the aperture stop is deformed by a mounting error, in addition to the field constant elliptical coma contribution, a field-conjugate, field-linear astigmatic contribution will also be introduced to the net aberration fields. On this basis, Ju et al. [23] quantify the effect of the trefoil deformation in an optical surface located away from the aperture stop and decentered from the optical axis, and quantitatively separate the effects of astigmatic and trefoil figure errors and misalignments for two-mirror telescopes. These works provide analytical analysis for describing and separating the effects of figure errors and misalignments. However, we are still lacking some knowledge concerning the interactions between the effects of figure errors and misalignments in the unobscured off-axis telescopes.

In this paper, we present a systematic and in-depth discussion of the aberration fields of off-axis two-mirror telescopes with offset pupil induced by lateral misalignments. Conceptually, we consider that an off-axis telescope with lateral misalignments is obtained by decentering the pupil of a parent on-axis system with the same misalignments while the other elements of the system (the aperture size of which are infinity) stay unchanged. Therefore, in this case, the off-axis system and its parent on-axis system have the same pupil size and misalignment parameters as well as some other optical parameters, except that the pupil of the off-axis system is decentered to achieve an unobscured configuration. Then we can analyze the aberration field characteristics of the misaligned off-axis telescopes based on the framework of NAT and a system level pupil coordinate transformation. We first derive an aberration function for the off-axis systems with lateral misalignments, and present a general description for the aberration field characteristics of them. Then we concentrate on some more specific characteristics of different aberration fields induced by lateral misalignments

Optics EXPRESS

particularly for the off-axis telescopes. Considering that the traditional off-axis two-mirror astronomical telescopes serve as an important tool in studying the solar activity and space weather, including the New Solar Telescope (NST) which has been in operation for years and the Advanced Technology Solar Telescope (ATST) [24] which is still under construction, we here use them as an example to discuss the specific aberration field characteristics in off-axis systems with lateral misalignments. Meanwhile, for a better explanation of this work, we reveal and illustrate the differences between the aberration fields of the misaligned off-axis systems and the on-axis ones, which can be interpreted as the effects of pupil decentration on the aberration fields of misaligned optical systems. Besides, after presenting the specific astigmatic and coma aberration field characteristics induced by lateral misalignments and further revealing their inherent relationships, we also make some quantitative discussions about the interactions between the effects of primary mirror astigmatic figure error and lateral misalignments for off-axis telescopes. While this work mainly uses the off-axis two-mirror telescopes to illustrate the aberration fields of off-axis telescopes, we will also present a brief discussion on the case of the off-axis TMA telescopes in each part of this paper from the Section 3. The knowledge of the aberration fields of off-axis systems induced by lateral misalignments presented in this paper can lead to some valuable insights for the optical design, alignment as well as active compensation and alignment of off-axis telescopes.

This paper is organized as follows. In Section 2, we derive the aberration function for the unobscured off-axis telescopes with lateral misalignments and present a general description of the aberration fields of them. In Section 3, the New Solar Telescope (NST) is taken as an example to discuss the specific astigmatic and coma aberration field characteristics in off-axis two-mirror telescopes and demonstrate the mathematical precision of the presented aberration function. Then we continue to reveal and explicate the inherent relationships between astigmatism and coma aberration fields and present some quantitative discussions concerning the active compensation and alignment strategies for active optics systems in off-axis two-mirror telescopes in Section 4. In Section 5, some other effects of lateral misalignments on the aberration fields of off-axis two-mirror telescopes are discussed, including medial focal surface and trefoil aberration. In Section 6, we summarize and conclude the paper.

2. Aberration function for misaligned off-axis telescopes with offset pupil

Explicit expression for the field dependence of each aberration type in rotationally symmetric systems

The net image plane aberration of rotationally symmetric optical systems consists of the sum of all the individual surface contributions, which can be descried by the wave aberration expansion in vector form, given by [11]

$$W = \sum_{j}\sum_{p}^{\infty}\sum_{n}^{\infty}\sum_{m}^{\infty}(W_{klm})_j\left(\vec{H}\cdot\vec{H}\right)^p\left(\vec{\rho}\cdot\vec{\rho}\right)^n\left(\vec{H}\cdot\vec{\rho}\right)^m, \tag{1}$$

where $k = 2p + m$ and $l = 2n + m$, $\vec{H}$ is the normalized field vector and $\vec{\rho}$ is the normalized pupil vector, $(W_{klm})_j$ denotes the aberration coefficient for a particular aberration type of surface j.

To facilitate the discussion in this paper, we here first change the form of Eq. (1) to explicitly express the field dependence of each aberration type which is defined historically by its dependence in the exit pupil. To this end, we need a vector identity presented below,

Optics EXPRESS

$$\left(\vec{H}\cdot\vec{\rho}\right)^m=\begin{cases}\sum_{t=0}^{\frac{(m-1)}{2}} a_m^{(t)}\left(\vec{H}\cdot\vec{H}\right)^t\left(\vec{\rho}\cdot\vec{\rho}\right)^t\vec{H}^{m-2t}\cdot\vec{\rho}^{m-2t}, & \text{if } m \text{ is odd.}\\ \sum_{t=0}^{\frac{m}{2}-1} a_m^{(t)}\left(\vec{H}\cdot\vec{H}\right)^t\left(\vec{\rho}\cdot\vec{\rho}\right)^t\vec{H}^{m-2t}\cdot\vec{\rho}^{m-2t}+\frac{a_m^{(m/2)}}{2}\left(\vec{H}\cdot\vec{H}\right)^{\frac{m}{2}}\left(\vec{\rho}\cdot\vec{\rho}\right)^{\frac{m}{2}}, & \text{if } m \text{ is even.}\end{cases}$$

(2)

where

$$a_m^{(t)}=\frac{1}{2^{m-1}}\binom{m}{t}=\frac{1}{2^{m-1}}\cdot\frac{m!}{t!(m-t)!}. \tag{3}$$

The derivation of Eq. (2) is presented in Appendix A.

Substituting Eq. (2) into Eq. (1), we can obtain

$$W=\sum_j\sum_p^{\infty}\sum_n^{\infty}\sum_m^{\infty}W'_{klmj}\left[\left(\vec{H}\cdot\vec{H}\right)^p\vec{H}^m\right]\cdot\left[\vec{\rho}^m\left(\vec{\rho}\cdot\vec{\rho}\right)^n\right], \tag{4}$$

where

$$W'_{klm}=\sum_{t=0}^{\frac{(q-m)}{2}}\frac{1}{1+\delta_{m0}}a_{m+2t}^{(t)}W_{kl(m+2t)},\ q=\min\{k,l\}, \tag{5}$$

and δ_{m0} is the Kronecker function ($\delta_{m0}=0$ if $m\neq 0$; $\delta_{m0}=1$ if $m=0$). This manipulation cannot only facilitate the discussion in the following parts of this section, but also has some physical relevance. For example, using Eqs. (4) and (5) we have

$$\begin{aligned}&W_{220}\left(\vec{H}\cdot\vec{H}\right)\left(\vec{\rho}\cdot\vec{\rho}\right)+W_{222}\left(\vec{H}\cdot\vec{\rho}\right)^2=W'_{220}\left(\vec{H}\cdot\vec{H}\right)\left(\vec{\rho}\cdot\vec{\rho}\right)+W'_{222}\vec{H}^2\cdot\vec{\rho}^2,\\ &W_{420}\left(\vec{H}\cdot\vec{H}\right)^2\left(\vec{\rho}\cdot\vec{\rho}\right)+W_{422}\left(\vec{H}\cdot\vec{H}\right)\left(\vec{H}\cdot\vec{\rho}\right)^2=W'_{420}\left(\vec{H}\cdot\vec{H}\right)^2\left(\vec{\rho}\cdot\vec{\rho}\right)+W'_{422}\left(\vec{H}\cdot\vec{H}\right)\vec{H}^2\cdot\vec{\rho}^2,\end{aligned} \tag{6}$$

where

$$\begin{aligned}W'_{220}&=W_{220}+\frac{1}{2}W_{222}=W_{220M},\ W'_{222}=\frac{1}{2}W_{222},\\ W'_{420}&=W_{420}+\frac{1}{2}W_{422}=W_{420M},\ W'_{422}=\frac{1}{2}W_{422},\end{aligned} \tag{7}$$

and here the subscript *M* means that the astigmatic aberration is measured with reference to the medial focal surface, upon which the minimum RMS wavefront error (WFE) can be measured [11, 14]. These conversions are the pivotal steps that led to the discovery of multi-nodal aberration field theory [11, 14].

Equation (4) can further be rewritten as

$$W=\sum_n^{\infty}\sum_m^{\infty}\vec{C}_{lm}\left(\vec{H}\right)\cdot\left[\vec{\rho}^m\left(\vec{\rho}\cdot\vec{\rho}\right)^n\right], \tag{8}$$

where $l=2n+m$, and

Optics EXPRESS

$$\vec{C}_{lm}\left(\vec{H}\right)=\sum_{j}\sum_{p}^{\infty}W'_{klmj}\left[\left(\vec{H}\cdot\vec{H}\right)^{p}\vec{H}^{m}\right]. \tag{9}$$

It can be seen that the aberrations of the rotationally symmetric systems have been categorized and grouped according to their dependence on the pupil vector. The field dependence of each aberration type, $\vec{C}_{lm}\left(\vec{H}\right)$, has been explicitly expressed. This expression can easily be related to the convention of optical testing where the wavefront at exit pupil is usually fitted to a Zernike polynomial as a representation of the measured wavefront. For example, when the aberrations through fifth order are considered ($m+n\le 3$), using vector multiplication of nodal aberration theory, Eq. (8) can be rewritten as

$$\begin{aligned}W=&C_{20}\rho^{2}+\begin{bmatrix}\vec{C}_{22,x}\\ \vec{C}_{22,y}\end{bmatrix}\cdot\begin{bmatrix}\rho^{2}\cos 2\phi\\ \rho^{2}\sin 2\phi\end{bmatrix}+\begin{bmatrix}\vec{C}_{31,x}\\ \vec{C}_{31,y}\end{bmatrix}\cdot\begin{bmatrix}\rho^{3}\cos\phi\\ \rho^{3}\sin\phi\end{bmatrix}+C_{40}\rho^{4}\\ &+\begin{bmatrix}\vec{C}_{33,x}\\ \vec{C}_{33,y}\end{bmatrix}\cdot\begin{bmatrix}\rho^{3}\cos 3\phi\\ \rho^{3}\sin 3\phi\end{bmatrix}+\begin{bmatrix}\vec{C}_{42,x}\\ \vec{C}_{42,y}\end{bmatrix}\cdot\begin{bmatrix}\rho^{4}\cos 2\phi\\ \rho^{4}\sin 2\phi\end{bmatrix}+\begin{bmatrix}\vec{C}_{51,x}\\ \vec{C}_{51,y}\end{bmatrix}\cdot\begin{bmatrix}\rho^{5}\cos\phi\\ \rho^{5}\sin\phi\end{bmatrix}+C_{60}\rho^{6},\end{aligned} \tag{10}$$

where the subscripts x, y represent two components of a vector, ϕ is the azimuthal angle in the exit pupil, and the field dependence of each aberration term is implicit in its coefficient for a certain field point. The piston and tilts terms are neglected in Eq. (10). The coefficients for the aberration terms can be easily related to the corresponding coefficients of the Fringe Zernike polynomials.

The explicit expression for the field dependence of each aberration in rotationally symmetric systems cannot only be easily related to the convention of optical testing, but also contribute to the discussion of the effects of lateral misalignments and pupil offset.

Aberration function for misaligned off-axis systems with offset pupils

When discussing the aberrations arising from an individual misaligned surface, the concept of local axis or local symmetry axis is important. The local axis is defined by the line that connects the center of curvature and the center of local entrance pupil for a particular surface. The aberration field associated with each surface is actually centered at the intersection of the local symmetry axis with the local object/image plane, which usually does not coincide with the field center (the intersection of optical axis ray (OAR) with the local object/image plane). As illustrated in Fig. 1, C represents the center of curvature for the nominal spherical surface (in black), C' represents the center of curvature for the misaligned surface (in gray), Q and E are the intersections of the OAR with the local object plane and local entrance pupil plane, respectively, i.e., they represent the local field center and pupil center, respectively. An arbitrary ray originates from the field point A and intersects with the pupil plane at point B. We can see that the aberration field center for this surface, P, does not coincide with the local field center, Q.

Optics EXPRESS

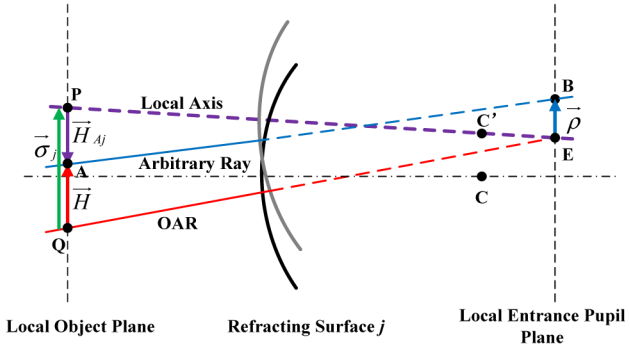

Fig. 1. Schematic representation for the concepts of shifted aberration field center and effective aberration field height.

In this case, the contribution of surface j to the overall aberration field is determined by the effective aberration field height of this surface [25], $\vec{H}_{Aj}$, as shown in Fig. 1. The effective aberration field height is defined as

$$\vec{H}_{Aj} = \vec{H} - \vec{\sigma}_j, \tag{11}$$

where the vector $\vec{\sigma}_j$ locates the shifted aberration field center for surface j, P, with reference to the field center, Q, as shown in Fig. 1. The magnitude and orientation of $\vec{\sigma}_j$ are directly related to the lateral misalignment parameters of surface j as well as the surfaces located before this surface [25].

The net aberration at exit pupil at any specific field point is still the sum of individual surface contribution while considering the fact that the individual-surface aberration contribution is now determined by its effective aberration field height. Therefore, in the presence of lateral misalignments, by replacing the field vector $\vec{H}$ with effective aberration field height $\vec{H}_{Aj}$ for each individual surface, the aberration function of the misaligned on-axis systems can be expressed as

$$W = \sum_{n}^{\infty}\sum_{m}^{\infty} \vec{C}_{lm}\left(\vec{H}_{Aj}\right)\cdot\left[\vec{\rho}^{\,m}\left(\vec{\rho}\cdot\vec{\rho}\right)^{n}\right], \tag{12}$$

where

$$\vec{C}_{lm}\left(\vec{H}_{Aj}\right) = \sum_{j}\sum_{p}^{\infty} W'_{klmj}\left[\left(\vec{H}_{Aj}\cdot\vec{H}_{Aj}\right)^{p}\vec{H}_{Aj}^{\,m}\right]. \tag{13}$$

It can be seen that after explicitly expressing the field dependence of each aberration type, the effects of lateral misalignments can easily be discussed. Referring to Eqs. (12-13) we can clearly see that no new aberration type is induced, but the field dependence of each aberration type, $\vec{C}_{lm}$, is modified.

After analytically accounting for the effects of lateral misalignments for on-axis systems, we begin to derive the aberration function for misaligned off-axis systems with offset pupils. Generally, an off-axis system with an offset pupil can be seen as an off-axis portion of a larger on-axis parent telescope, as illustrated in Fig. 2(a), where the large circle represents the pupil of the on-axis parent telescope and the small circle in grey represents the pupil of the off-axis telescope.

The relation between the coordinate of the off-axis portion and its parent on-axis pupil in Fig. 2(a) can be given by

Optics EXPRESS

$$\vec{\rho} = b\vec{\rho}' + \vec{s}, \tag{14}$$

where $\vec{\rho}$ denotes the on-axis pupil vector normalized by the half aperture size of the on-axis parent pupil, $\vec{\rho}'$ is the off-axis pupil vector normalized by the half aperture size of the off-axis pupil, $\vec{s}$ represents the location of the off-axis pupil normalized by the half aperture size of the on-axis parent pupil, and b represents the scale factor of the aperture size of the off-axis pupil relative to the parent on-axis pupil.

The wavefront error in the off-axis portion can still be expressed using the aberration function for the parent on-axis system as

$$W = \sum_{n}^{\infty}\sum_{m}^{\infty} \vec{C}_{lm}\left(\vec{H}_{Aj}\right)\cdot\left[\vec{\rho}^{m}\left(\vec{\rho}\cdot\vec{\rho}\right)^{n}\right], \qquad \vec{\rho}\in D, \tag{15}$$

where D represents region of the off-axis portion. However, this expression cannot be directly seen as the aberration function of the off-axis system, for wave aberration is usually measured at exit pupil with corresponding normalized pupil coordinate. Using the pupil coordinate transformation between the parent on-axis pupil and the off-axis pupil, the wavefront error of the off-axis system in the presence of lateral misalignments can be rewritten as

$$W = \sum_{n}^{\infty}\sum_{m}^{\infty} \vec{C}_{lm}\left(\vec{H}_{Aj}\right)\cdot\left\{\left(b\vec{\rho}'+\vec{s}\right)^{m}\left[\left(b\vec{\rho}'+\vec{s}\right)\cdot\left(b\vec{\rho}'+\vec{s}\right)\right]^{n}\right\}, \tag{16}$$

where it can be seen that the final measurement is done in the corresponding pupil coordinate of the off-axis system. Therefore, this expression can be seen as the aberration function for the misaligned off-axis system, which can analytically describe how the total aberration of the off-axis system changes with its field coordinate, pupil coordinate as well as misalignments.

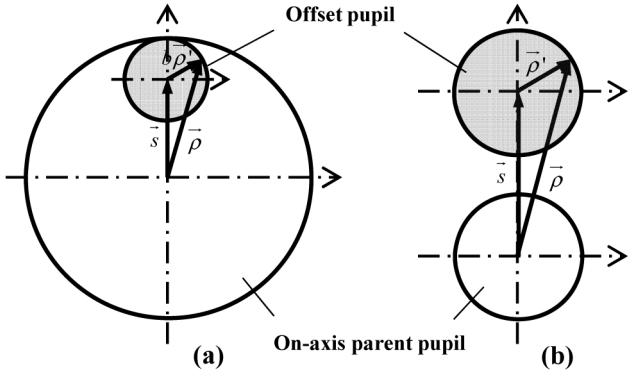

Fig. 2. Schematic representation for two conceptual methods of obtaining an off-axis configuration from an on-axis parent system. (a) The off-axis system can be seen as an off-axis portion of a larger on-axis parent system. (b) The off-axis system is obtained by decentering the pupil of an on-axis system while the other elements of the system (the aperture size of which are infinity) stay unchanged. These two methods are essentially equivalent.

The concept that an off-axis system can be seen as an off-axis portion of a larger on-axis parent system is easy to understand. This concept has been widely used for optical fabrication and testing of off-axis surfaces. However, this concept is not very suitable for the discussion of this paper. It can be seen in Eq. (16) that the aberration of the off-axis systems depends on too many factors, including the aberration function of the parent system, the pupil dencentration vector as well as the pupil scale factor, which is unfavorable for us to reveal some underlying rules or deep level knowledge. Therefore, we here use another conceptual

Optics EXPRESS

method of obtaining an off-axis configuration proposed in [26], i.e., only the pupil of the on-axis parent system is decentered, while the other elements of the system (the aperture size of which are infinity) stay unchanged, as illustrated in Fig. 2(b), where the circle in grey represents the off-axis pupil, which has the same pupil size as the on-axis parent pupil, and all the three vectors are normalized by the half aperture size of the on-axis parent pupil. Not that the off-axis system and its on-axis parent system have the same misalignment parameters in this case.

While in this case the vector $\vec{\rho}$ exceeds the normalized radius, its origin still coincides with the origin of the on-axis pupil coordinate. Therefore, it can still represent the coordinate of the on-axis parent pupil. In this case, the coordinate transformation between the offset pupil and the on-axis parent pupil can be expressed as

$$\vec{\rho} = \vec{\rho}' + \vec{s}. \tag{17}$$

Similarly, the aberration function of the off-axis system can be obtained by using the aberration function of the on-axis parent system,

$$W = \sum_{n}^{\infty}\sum_{m}^{\infty} \vec{C}_{lm}\left(\vec{H}_{Aj}\right)\cdot\left\{\left(\vec{\rho}' + \vec{s}\right)^{m}\left[\left(\vec{\rho}' + \vec{s}\right)\cdot\left(\vec{\rho}' + \vec{s}\right)\right]^{n}\right\}. \tag{18}$$

It can be seen that the aberration function of the off-axis system only depends on the aberration function of its parent system with a same pupil size and the pupil decentration vector. We can easily infer that, to obtain an unobscured off-axis configuration, we should have that $|\vec{s}|>1$, where $|\vec{s}|$ is the magnitude of the pupil decentration vector, and usually $|\vec{s}|$ is about 2. In effect, the two conceptual methods of obtaining an off-axis configuration from an on-axis system are equivalent. The on-axis pupil in the Fig. 2(b) can be seen as an on-axis portion of the on-axis pupil in Fig. 2(a), which has the same aperture size as the off-axis portion.

Deriving the aberration function for an off-axis system using an on-axis system with the same pupil size cannot only make the form of the aberration function more simple and intuitive, but also facilitate the discussion of the differences between the misalignment-induced aberration fields of the unobscured off-axis system and its on-axis parent system, which are purely induced by the effects of pupil offset (i.e., have nothing to do with the pupil size).

Besides, there is a question in the derivation of the aberration function for off-axis systems, i.e., while both lateral misalignments and pupil decenter can make the pupil be off-axis, why we use different methods to discuss their effects? While the effects of lateral misalignments and pupil decenter bear some similarities, however, they still have some fundamental differences. On the one hand, the magnitude of the pupil decenter used to obtain an unobscured configuration is far larger than that induced by lateral misalignments. Therefore, when the pupil is decentered to obtain an unobscured configuration, the line that connects the local pupil center and the center of curvature for an individual surface can no longer be seen as the local symmetry axis for this surface. Consequently, the effects of pupil decenter cannot directly be discussed using nodal aberration theory. On the other hand, another difference between the effects of pupil decenter and misalignments is that the former does not change the relative position between different optical surfaces. In other words, it does not change the intersection of an arbitrary ray with the pupil plane. What does change is the definition of the origin of the pupil coordinate. Therefore, we use a system level pupil coordinate transformation to include the effects of pupil decenter and derive the aberration function for misaligned off-axis systems.

Optics EXPRESS

General descriptions for the misalignment-induced aberration fields of off-axis systems

Before analyzing the misalignment-induced aberration field characteristics of off-axis systems, we should explicitly express the field dependencies of different aberration types. To this end, we need to expand Eq. (18), convert the pupil dependence of each term into existing aberration types and group the aberration coefficients according to their pupil dependence. While it is quite hard to derive the exact expression for the field dependence of each aberration type, which is generally an infinite sum, we can derive this expression under certain specific conditions, which can help us to obtain some general descriptions for the misalignment-induced aberration fields of off-axis systems.

According to the binomial theorem, each term in Eq. (18) can be expanded as

$$\begin{aligned}
&\vec{C}_{lm}\cdot\left(\vec{\rho}+\vec{s}\right)^{m}\left[\left(\vec{\rho}+\vec{s}\right)\cdot\left(\vec{\rho}+\vec{s}\right)\right]^{n}\\
&=\left[\sum_{f=0}^{m}\binom{m}{f}\vec{C}_{lm}\cdot\vec{s}^{\,m-f}\,\vec{\rho}^{\,f}\right]\left[\sum_{g=0}^{n}\sum_{h=0}^{n-g}\binom{n}{g}\binom{n-g}{h}2^{h}\left(\vec{\rho}\cdot\vec{\rho}\right)^{g}\left(\vec{s}\cdot\vec{\rho}\right)^{h}\left(\vec{s}\cdot\vec{s}\right)^{n-g-h}\right] \qquad (19)\\
&=\sum_{f=0}^{m}\sum_{g=0}^{n}\sum_{h=0}^{n-g}K_{fgh}\left(\vec{s}\cdot\vec{s}\right)^{n-g-h}\left[\left(\vec{s}^{\,*}\right)^{m-f}\vec{C}_{lm}\cdot\vec{\rho}^{\,f}\right]\left(\vec{s}^{\,h}\cdot\vec{\rho}^{\,h}\right)\left(\vec{\rho}\cdot\vec{\rho}\right)^{g},
\end{aligned}$$

where

$$K_{fgh}=\sum_{t=0}^{\frac{q'-h}{2}}\frac{1}{1+\delta_{h0}}a_{h+2t}^{(t)}\binom{m}{f}\binom{n}{g-t}\binom{n-(g-t)}{h+2t}2^{h+2t},\quad q'=\min\left\{2g+h,2n-(2g+h)\right\}. \qquad (20)$$

Here the vector identity similar to Eq. (2) has been used to convert the aberration terms with $\left(\vec{s}\cdot\vec{\rho}\right)^{h}$ to those with $\left(\vec{s}^{\,h}\cdot\vec{\rho}^{\,h}\right)$.

Then referring to another vector identity, the derivation of which is presented in Appendix B,

$$2\left(\vec{A}\cdot\vec{C}^{\,p}\right)\left(\vec{B}\cdot\vec{C}^{\,q}\right)=\begin{cases}\vec{A}\vec{B}\cdot\vec{C}^{\,p+q}+\left(\vec{A}\vec{B}^{\,*}\cdot\vec{C}^{\,p-q}\right)\left(\vec{C}\cdot\vec{C}\right)^{q}, & p>q,\\ \vec{A}\vec{B}\cdot\vec{C}^{\,p+q}+\left(\vec{A}^{\,*}\vec{B}\cdot\vec{C}^{\,q-p}\right)\left(\vec{C}\cdot\vec{C}\right)^{p}, & p<q,\\ \vec{A}\vec{B}\cdot\vec{C}^{\,2p}+\left(\vec{A}\cdot\vec{B}\right)\left(\vec{C}\cdot\vec{C}\right)^{p}, & p=q,\end{cases} \qquad (21)$$

where p and q are positive integers and $\vec{A}^{\,*}$ represents the conjugate vector of $\vec{A}$, we can convert each term in Eq. (19) into a series of existing aberration types.

Utilizing Eqs. (18-21), when only the 3rd-order aberrations of the on-axis parent system are considered, i.e., $m+n\le 2$, the aberrations of the off-axis system through third order can be expressed as

$$W^{(U)}=C_{20}^{(U)}\cdot\left(\vec{\rho}\cdot\vec{\rho}\right)+\vec{C}_{22}^{(U)}\cdot\vec{\rho}^{\,2}+\vec{C}_{31}^{(U)}\cdot\vec{\rho}\left(\vec{\rho}\cdot\vec{\rho}\right)+C_{40}^{(U)}\cdot\left(\vec{\rho}\cdot\vec{\rho}\right)^{2}, \qquad (22)$$

where

Optics EXPRESS

$$
\begin{aligned}
C_{20}^{(U)} &= C_{20} + 2\vec{C}_{31}\cdot\vec{s} + 4C_{40}\left(\vec{s}\cdot\vec{s}\right),\\
\vec{C}_{22}^{(U)} &= \vec{C}_{22} + \vec{C}_{31}\vec{s} + 2C_{40}\vec{s}^{2},\\
\vec{C}_{31}^{(U)} &= \vec{C}_{31} + 4C_{40}\vec{s},\\
C_{40}^{(U)} &= C_{40},
\end{aligned}
\tag{23}
$$

and the super-script (U) indicates that the coefficients are for the aberrations in unobscured off-axis systems. Equations (22-23) are named as the "3rd-order model" for describing the aberration fields of off-axis systems with lateral misalignments in the following parts.

When the aberrations through fifth order of the on-axis parent system are considered, i.e., $m+n\le 3$, the aberrations of the off-axis system through fifth order can be expressed as

$$
\begin{aligned}
W^{(U)} = C_{20}^{(U)}\cdot\left(\vec{\rho}\cdot\vec{\rho}\right) + \vec{C}_{22}^{(U)}\cdot\vec{\rho}^{2} + \vec{C}_{31}^{(U)}\cdot\vec{\rho}\left(\vec{\rho}\cdot\vec{\rho}\right) + C_{40}^{(U)}\cdot\left(\vec{\rho}\cdot\vec{\rho}\right)^{2} +\\
\vec{C}_{33}^{(U)}\cdot\vec{\rho}^{3} + \vec{C}_{42}^{(U)}\cdot\vec{\rho}^{2}\left(\vec{\rho}\cdot\vec{\rho}\right) + \vec{C}_{51}^{(U)}\cdot\vec{\rho}\left(\vec{\rho}\cdot\vec{\rho}\right)^{2} + \vec{C}_{60}^{(U)}\cdot\left(\vec{\rho}\cdot\vec{\rho}\right)^{3},
\end{aligned}
\tag{24}
$$

where

$$
\begin{aligned}
C_{20}^{(U)} &= C_{20} + 2\vec{C}_{31}\cdot\vec{s} + 4C_{40}\left(\vec{s}\cdot\vec{s}\right) + 3\left(\vec{C}_{42}\cdot\vec{s}^{2}\right) +\\
&\quad 6\left(\vec{s}\cdot\vec{s}\right)\left(\vec{s}\cdot\vec{C}_{51}\right) + 9C_{60}\left(\vec{s}\cdot\vec{s}\right)^{2},\\
\vec{C}_{22}^{(U)} &= \vec{C}_{22} + \vec{C}_{31}\vec{s} + 2C_{40}\vec{s}^{2} + 3\vec{C}_{33}\vec{s}^{*} + 3\left(\vec{s}\cdot\vec{s}\right)\vec{C}_{42} +\\
&\quad 2\left(\vec{s}\cdot\vec{s}\right)\vec{s}\vec{C}_{51} + 2\left(\vec{s}\cdot\vec{C}_{51}\right)\vec{s}^{2} + 6C_{60}\left(\vec{s}\cdot\vec{s}\right)\vec{s}^{2},\\
\vec{C}_{31}^{(U)} &= \vec{C}_{31} + 4C_{40}\vec{s} + 3\vec{C}_{42}\vec{s}^{*} + 4\left(\vec{s}\cdot\vec{s}\right)\vec{C}_{51} +\\
&\quad 4\left(\vec{s}\cdot\vec{C}_{51}\right)\vec{s} + \vec{s}^{2}\vec{C}_{51}^{*} + 18C_{60}\left(\vec{s}\cdot\vec{s}\right)\vec{s},\\
C_{40}^{(U)} &= C_{40} + 3\left(\vec{s}\cdot\vec{C}_{51}\right) + 9C_{60}\left(\vec{s}\cdot\vec{s}\right),\\
\vec{C}_{33}^{(U)} &= \vec{C}_{33} + \vec{C}_{42}\vec{s} + \vec{C}_{51}\vec{s}^{2} + 2C_{60}\vec{s}^{3},\\
\vec{C}_{42}^{(U)} &= \vec{C}_{42} + 2\vec{C}_{51}\vec{s} + 6C_{60}\vec{s}^{2},\\
\vec{C}_{51}^{(U)} &= \vec{C}_{51} + 6C_{60}\vec{s},\\
C_{60}^{(U)} &= C_{60}.
\end{aligned}
\tag{25}
$$

All these aberration coefficients, $\vec{C}_{lm}$ and $\vec{C}_{lm}^{(U)}$, are a function of the effective field height for each individual surface of the parent on-axis system, $\vec{H}_{Aj}$, which are directly related to the misalignment parameters. Equations (24-25) are named as the "5th-order model" for describing the aberration fields of off-axis systems with lateral misalignments in the following parts of this paper. The piston and tilt terms are neglected in Eqs. (22-25).

It is shown that under some specific conditions the aberrations of an off-axis system in the presence of misalignments can be clearly expressed using the aberrations of its on-axis parent system and pupil decentration vector. Compared to the field dependence of each aberration type in misaligned on-axis systems, the field dependence of each aberration type in misaligned off-axis systems is further modified by the pupil decentration vector. Here we

Optics EXPRESS

continue to stress that the off-axis system has the same pupil size and misalignment parameters as its on-axis parent system. Comparing Eqs. (22-25) with Eqs. (12-13) we can obtain some general descriptions mainly concerning the differences between the misalignment-induced aberration fields of the off-axis systems and on-axis systems, which is due to the effects of pupil decentration:

(1) The off-axis systems are more sensitive to misalignments compared to their parent on-axis systems with a same aperture size. Each aberration term of the off-axis systems includes contributions generated by the higher-order aberrations of the on-axis parent systems through pupil coordinate transformation, apart from the same aberration of the on-axis parent systems. Therefore, the total misalignment-induced aberrations of the off-axis systems are larger than their parent on-axis systems.

(2) The sensitivity of off-axis systems to misalignments is associated with the directions of the misalignments. One of the reasons is that the lower-order aberrations of the off-axis systems include some contributions with the factor of $\left(\vec{s}\cdot\vec{C}_{lm}\right)$. The direction of $\vec{s}$ is constant while the direction of $\vec{C}_{lm}$ is dependent on the directions of misalignments. Considering that the dot product of two vectors is related to the angle between them, therefore, the directions of the misalignments can impact the magnitude of the misalignment-induced aberrations. The underlying cause is that when the pupil is offset, the rotational symmetry of the previous on-axis system is broken, and only a plane symmetric property of the system is maintained.

(3) In off-axis systems, the effects of lateral misalignments couple more tightly with axial misalignments than in on-axis systems. Generally, in on-axis systems, axial misalignments mainly induce rotationally symmetric aberrations, such as defocus, and have little effect on non-rotationally symmetric aberrations, such as astigmatism and coma, while lateral misalignments mainly affect the non-rotationally symmetric aberrations. However, through pupil coordinate transformation, those rotationally symmetric aberrations with high-order pupil dependence can generate lower-order non-rotationally symmetric ones, and those non-rotationally symmetric aberrations with higher-order pupil dependence can generate lower-order rotationally symmetric ones, making the effects of lateral and axial misalignments couple more tightly together in determining the total aberration fields.

(4) Each aberration of the parent on-axis system can generate a series of lower-order aberrations in the off-axis system, making different aberrations can have deeply inherent relationships in off-axis systems with misalignments. The inherent relationships between astigmatism and coma will be taken as an important example to demonstrate this standpoint in the following parts of this paper.

All these arguments are important for an in-depth understanding of the misalignment-induced aberrations of unobscured off-axis telescopes with offset pupil. They will be further mentioned and illustrated in the rest chapters of this paper where the New Solar Telescope (NST), a famous off-axis two-mirror telescope, will be taken as an example to discuss the misalignment-induced aberrations in off-axis telescopes.

However, these general descriptions are not enough. In the following parts, on the one hand, the emphasis will be shifted to some more specific aberration field characteristics induced by lateral misalignments for off-axis two-mirror telescopes, which can lead to some theoretical guidance for the optical design, alignment and active alignment of off-axis systems; on the other hand, some important quantitative discussions are also presented.

Optics EXPRESS

3. Coma and astigmatic aberration fields of off-axis two-mirror telescopes induced by lateral misalignments

From this section, we will begin to present some specific misalignment-induced aberration field characteristics of off-axis two-mirror telescopes with offset pupil, including coma and astigmatic aberration fields. On the one hand, we use the 3rd-order model to discuss the nodal properties of the coma and astigmatic aberration fields in misaligned off-axis two-mirror telescopes. Specifically, we find that the astigmatic aberration field in misaligned off-axis two-mirror telescopes is very different from that in the on-axis ones. On the other hand, we use the ray tracing data to demonstrate the correctness and accuracy of the 3rd-order model and the 5th-order model for describing the coma and astigmatic aberration fields. The discrepancies between the three sets of data are also explicated.

Coma aberration field of off-axis two-mirror telescopes induced by lateral misalignments

Referring to Eqs. (22-23), for the off-axis two-mirror telescopes in the presence of lateral misalignments, the coma aberration fields can be expressed as

$$W_{Coma}^{(U)} = \vec{C}_{31}^{(U)} \cdot \vec{\rho}\left(\vec{\rho}\cdot\vec{\rho}\right), \tag{26}$$

where

$$\begin{aligned} \vec{C}_{31}^{(U)} &= \left(\vec{C}_{31} + 4C_{40}\vec{s}\right) \\ &= \sum_j \left[W_{131j}\left(\vec{H} - \vec{\sigma}_j\right) + 4W_{040j}\vec{s} \right] \\ &= W_{131}\vec{H} + 4W_{040}\vec{s} - \vec{A}_{131}^{(P)}, \end{aligned} \tag{27}$$

with $\vec{A}_{131}^{(P)} = \sum_j W_{131j}\vec{\sigma}_j$. W_{klmj} represents the certain aberration coefficient for surface j of the on-axis parent system with a same aperture size, and the super-script (P) indicates that the field displacement vector particularly for the parent on-axis system. Here only the 3rd-order aberrations of the on-axis parent system are considered in the derivation of $\vec{C}_{31}^{(U)}$ (i.e., only the 3rd-order model is used here). Considering that for traditional two-mirror telescopes the 3rd-order coma is not corrected in the nominal state, i.e., $W_{131} \neq 0$, therefore, according to Eq. (27) we can see that the coma aberration field can be as a combination of a field-linear component and a field-constant component, which is similar with the coma aberration field in misaligned on-axis two systems.

Then we begin to use the 3rd-order model to discuss the nodal properties of the coma aberration field in off-axis two-mirror telescopes. Equation (26) can be rewritten as

$$W_{Coma}^{(U)} = W_{131}\left(\vec{H} - \frac{\vec{A}_{131}^{(P)} - 4W_{040}\vec{s}}{W_{131}}\right)\cdot\vec{\rho}\left(\vec{\rho}\cdot\vec{\rho}\right). \tag{28}$$

While coma is not corrected in the nominal state for traditional two-mirror telescopes, however, it is still very small for guaranteeing the optical performance across the field of view. In the presence of misalignments, the magnitude of $\left|\vec{A}_{131}^{(P)}\right|$ can be far larger than $\left|W_{131}\right|$,

Optics EXPRESS

i.e., $\left|\vec{A}_{131}^{(P)}\right| >> W_{131}$. The underlying reason for this is that the coma aberration contributed from the spherical base sphere, $W_{131j}^{(sph)}$, and the aspheric departure, $W_{131j}^{(asph)}$, of an individual surface are far larger than their total sum in the nominal state, W_{131}, for large astronomical telescopes. Take the NST as example, $W_{131} = -0.02\lambda(\lambda = 500\text{nm})$, while the coma aberration coefficients associated with the spherical base sphere and the aspheric departure of the secondary mirror are $W_{131,SM}^{(sph)} = 4.39\lambda$, and $W_{131,SM}^{(sph)} = 4.63\lambda$ (obtained at a field angle of 0.03°), respectively. In the misaligned state, the aberration field center for each individual surface no longer coincides, which can result in a relatively large coma aberration. This conclusion will also be used when discussing the astigmatic aberration field in off-axis two-mirror telescopes with lateral misalignments.

Furthermore, the spherical aberration is nearly corrected, and we here neglect it. Therefore, in the misaligned state, it is very likely that

$$\left|\frac{\vec{A}_{131}^{(P)} - 4W_{040}\vec{s}}{W_{131}}\right| >> 1, \tag{29}$$

which means that the node of the coma aberration field for off-axis two-mirror telescopes usually lies far away from the field of view in the presence of misalignments.

The NST is used to demonstrate the coma aberration field characteristics presented above. The specific optical prescription and layout of this telescope are presented in the Appendix C. Note that for this off-axis telescope, the pupil decentration vector is given by $\vec{s} = [0, -2.3]^T$. The full field display (FFD) over a $\pm 0.03°$ field of view for the misalignment-induced coma (Z7/Z8) of this off-axis telescope and its parent telescope with the same aperture size are shown in Fig. 3. Here we use the primary mirror as the reference and the specific misalignment parameters of the secondary mirror are XDE_{SM} = 0.04mm, YDE_{SM} = 0.02mm, ADE_{SM} = 0.002°, and BDE_{SM} = –0.005°. XDE_{SM} and YDE_{SM} are the secondary mirror vertex decenters in the x-z and y-z plane, respectively, and BDE_{SM} and ADE_{SM} are the secondary mirror tip-tilts in the x-z and y-z plane, respectively. In Fig. 3 the length of the comet indicates the magnitude of coma and the head of the comet points to the direction of coma.

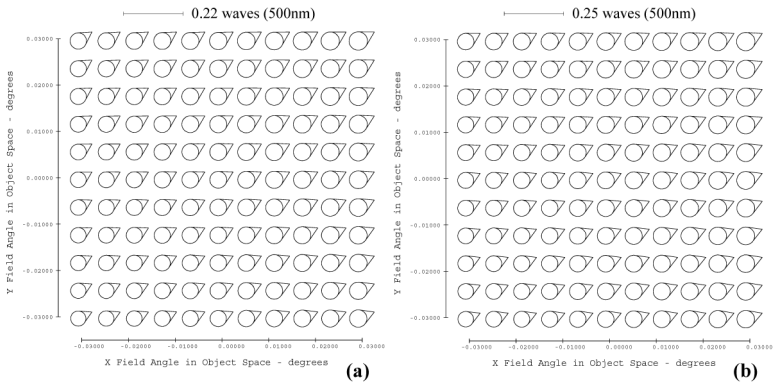

Fig. 3. FFDs for coma (Z7/Z8) in the NST (a) and its parent on-axis telescope with the same aperture size (b) in the presence of the same lateral misalignments specified above. It can be seen that both of them are a combination of a field-linear component and a field-constant component. Besides, no node lies in the field of view.

Optics EXPRESS

We should point out that all the FFDs presented in this paper are directly obtained from the optical simulation software CODE V, not custom-built. We can see that the coma aberration field in the NST with lateral misalignments is actually a combination of a field-linear component and a field-constant component, and the node of it lies far away from the field of view, which agree with the descriptions for the coma aberration field presented above.

For off-axis TMA telescopes, the 3rd-order coma is corrected, i.e., $W_{131}=0$. It can be inferred from Eqs. (26)-(27) that the misalignment-induced coma aberration field in off-axis TMA telescopes is field-constant. Therefore, no node is located in the field of view.

After presenting a qualitative description of the coma aberration field for off-axis two-mirror telescopes with lateral misalignments, we here continue to further present a quantitative discussion. As mentioned above, only the 3rd-order model is use in the derivation of coma aberration field, $\vec{C}_{31}^{(U)}$. The mathematical precision of this expression should be verified by comparing the results of this expression to the ray tracing data. On the other hand, we also present the 5th-order model (Eqs. (24)-(25)) for describing each aberration field in off-axis systems with misalignments. Comparing the accuracy of the 3rd-order model and the 5th-order model can further help us to understand where the discrepancies between our analytic expression and the ray tracing data come from.

We use the primary mirror as the reference coordinate system, which also serves as the aperture stop. This means that both of the field center displacement vectors associated with the spherical base curve and the aspheric departure of the primary mirror are equivalent to zero, i.e., $\vec{\sigma}_{PM}^{(sph)}=0$, and $\vec{\sigma}_{PM}^{(asph)}=0$. Therefore, those aberration coefficients associated with the spherical base curve and the aspheric departure of the primary mirror are not needed in the calculation. The 3rd-order aberration coefficients of the system and those associated with the spherical base curve and the aspheric departure of the secondary mirror are presented in Appendix D. On the other hand, we find that for the NST with a very small field of view, apart from W_{060} and the 5th-order aperture coma aberration coefficients associated with the spherical base sphere and the aspheric departure of the secondary mirror, $W_{151,SM}^{(sph)}$ and $W_{151,SM}^{(asph)}$, all the other 5th-order aberration coefficients needed in the calculation are particularly small and we can neglect them. The specific values of these three aberration coefficients are $W_{060}=-0.00008\lambda(\lambda=500\,\text{nm})$, $W_{151,SM}^{(sph)}=-0.04660\lambda$, $W_{151,SM}^{(asph)}=-0.04924\lambda$. Note that while $W_{151,SM}^{(sph)}\neq 0$ and $W_{151,SM}^{(asph)}\neq 0$, we find the total aberration coefficient for the 5th-order aperture coma of system W_{151} is far smaller than 0.0001λ, so we neglect it. With these aberration coefficients we can now make a comparison between the ray tracing data and our 3rd-order model and 5th-order model.

In the presence of the misalignments specified above, the Fringe Zernike coefficients for coma (C_7/C_8) at three field points ((0,0), (0.03°,0.03°), (0.03°,-0.03°)) obtained directly from the simulation software and calculated with the 3rd and 5th model are presented in Table 1.

Table 1. Verification for the Coma Aberration Field in the Misaligned NST

	(0,0)		(0.03°,0.03°)		(0.03°,-0.03°)	
	C_7	C_8	C_7	C_8	C_7	C_8
Ray Tracing	-0.0827	-0.0435	-0.0894	-0.0500	-0.0893	-0.0365
3rd-order Model	-0.0975	-0.0676	-0.1042	-0.0741	-0.1042	-0.0607
5th-order Model	-0.0808	-0.0388	-0.0876	-0.0453	-0.0876	-0.0318

We can see from Table 1 that the 3rd-order model can roughly represent the general characteristics of the coma aberration field in misaligned off-axis two-mirror telescopes, i.e.,

Optics EXPRESS

the coma aberration field can be seen as a combination of a small field-linear component and a large field-constant component. However, the 3rd-order model is far from accurate.

By contrast, the 5th-order model is more accurate. It will be seen in the later parts of this section that while those 5th-order aberration coefficients considered in this paper (W_{060}, $W_{151,SM}^{(sph)}$ and $W_{151,SM}^{(asph)}$) are still very small, their effects can be greatly magnified through pupil coordinate transformation.

However, it can be recognized that there still exist some discrepancies between the ray tracing data and those calculated using 5th-order model. Apparently this is not because we neglect some 5th-order order aberration coefficients. We neglect them because we find their effects are far too small for us to consider them. In effect, these discrepancies are mainly due to those 7th- and more higher-order aberrations of the parent on-axis system that are not considered in the 5th-order model. This question will be further discussed in the following part of this section.

Astigmatic aberration field of off-axis two-mirror telescopes induced by lateral misalignments

Referring to Eqs. (22)-(23), the astigmatic aberration field in off-axis two-mirror telescopes with lateral misalignments can be expressed as

$$W_{AST}^{(U)} = \vec{C}_{22}^{(U)} \cdot \vec{\rho}^2, \tag{30}$$

where

$$\begin{aligned} \vec{C}_{22}^{(U)} &= \vec{C}_{22} + \vec{C}_{31}\vec{s} + 2C_{40}\vec{s}^2 \\ &= \sum_j \left[\frac{1}{2} W_{222j} \left(\vec{H} - \vec{\sigma}_j \right)^2 + W_{131j} \left(\vec{H} - \vec{\sigma}_j \right) \vec{s} + 2W_{040j} \vec{s}^2 \right]. \\ &= \frac{1}{2} W_{222} \vec{H}^2 + \left(W_{131}\vec{s} - \vec{A}_{222}^{(P)} \right) \vec{H} + \left(2W_{040}\vec{s}^2 + \frac{1}{2}\vec{B}_{222}^{2(P)} - \vec{A}_{131}^{(P)}\vec{s} \right) \end{aligned} \tag{31}$$

with

$$\vec{A}_{222}^{(P)} = \sum_j W_{222j} \vec{\sigma}_j, \quad \vec{B}_{222}^{2(P)} = \sum_j W_{222j} \vec{\sigma}_j^2, \tag{32}$$

For simplicity, here only the 3rd-order aberrations of the on-axis parent system are considered in the derivation of $\vec{C}_{22}^{(U)}$, which can help to grasp the main points. Considering that the spherical aberration is well corrected for most astronomical telescopes and the term $\vec{B}_{222}^{2(P)}$, which is proportional to the misalignment squared, can also be neglected for misalignment level perturbations, the field dependence of the astigmatism in misaligned off-axis two-mirror telescopes can further be rewritten as

$$\vec{C}_{22}^{(U)} = \frac{1}{2} W_{222} \vec{H}^2 + \left(W_{131}\vec{s} - \vec{A}_{222}^{(P)} \right) \vec{H} + \left(-\vec{A}_{131}^{(P)}\vec{s} \right). \tag{33}$$

Compared to the astigmatic aberration field in misaligned on-axis two-mirror systems [17], we can see that two additional astigmatic components are added to the net aberration field of misaligned off-axis systems, i.e., a small field-linear component, $W_{131}\vec{s} \cdot \vec{\rho}^2$, and a relatively large field-constant component, $-\vec{A}_{131}^{(P)}\vec{s} \cdot \vec{\rho}^2$. In effect, as will be seen below, the field-

Optics EXPRESS

constant one represents the main difference between the misalignment-induced astigmatic aberration field in the on-axis telescopes and the off-axis ones.

For traditional two-mirror telescopes, $W_{222} \neq 0$, and therefore it may seem that the astigmatism in the off-axis ones is bi-nodal in the presence of misalignments. However, this does mean that the nodes of the astigmatism are located in the field of view. As will be demonstrated in the following parts, actually there are no nodes located in the field of view.

According to the Seidel formula, for on-axis systems we have that

$$W_{222j}^{(sph)} = \frac{\bar{i}_j}{i_j} W_{131j}^{(sph)}, \quad W_{222j}^{(asph)} = \frac{\bar{y}_j}{y_j} W_{131j}^{(asph)}, \tag{34}$$

where the super-scripts (sph) and $(asph)$ indicate that these aberration coefficients are for the spherical base sphere and the aspheric departure, respectively, $\bar{i}_j$ and i_j are the chief-ray incident angle and marginal-ray incident angle at surface *j*, respectively, and $\bar{y}_j$ and y_j are the chief-ray height and marginal-ray height at the surface *j*, respectively. In general, for the mirrors in large astronomical telescope systems with a relatively small field of view, we can have that $\left|\bar{i}_j\right| << \left|i_j\right|$, $\left|\bar{y}_j\right| << \left|y_j\right|$ (here $|\cdot|$ represents the absolute value operator). Referring to Eq. (34) we can know that the coma aberration coefficient for an individual surface is usually much larger than astigmatic aberration coefficient, which indicates that the magnitude of $\vec{A}_{131}^{(P)}$, $\left|\vec{A}_{131}^{(P)}\right|$, is usually much larger than the magnitude of $\vec{A}_{222}^{(P)}$, $\left|\vec{A}_{222}^{(P)}\right|$. Besides, for off-axis astronomical telescopes with unobscured pupil, we at least have $\left|\vec{s}\right| > 1$ and usually $\left|\vec{s}\right|$ is about 2 ($\left|\vec{s}\right|$ represents the ratio of the magnitude of the pupil decenter to the half pupil size). Consequently, in general we can have that

$$\left|\vec{A}_{131}^{(P)}\vec{s}\right| >> \left|\vec{A}_{222}^{(P)}\right|. \tag{35}$$

On the other hand, while the astigmatism and coma are not corrected for traditional astronomical two-mirror telescopes, however, actually they are very small for guaranteeing the optical performance across the typically small field of view. As demonstrated in the previous part of the section, in the misaligned state it is very likely that $\left|\vec{A}_{131}^{(P)}\right| >> W_{131}$. Therefore, in the field of view ($\left|\vec{H}\right| \le 1$), we can have that

$$\left|\frac{1}{2}W_{222}\vec{H}^2 + \left(W_{131}\vec{s} - \vec{A}_{222}^{(P)}\right)\vec{H}\right| \le \left|\frac{1}{2}W_{222}\right| + \left|W_{131}\vec{s}\right| + \left|\vec{A}_{222}^{(P)}\right| << \left|\vec{A}_{131}^{(P)}\vec{s}\right|, \tag{36}$$

which indicates that in general no node is existed in the field of view. In other words, in the presence of misalignments, the magnitude of the field-constant astigmatism component is far larger than the field-linear component and the field-quadratic component, making the nodes of the astigmatism lie far away from the field of view. This is very different from the astigmatic aberration field in misaligned on-axis two-mirror telescopes.

To demonstrate the astigmatic aberration field characteristics presented above, the full field displays (FFDs) for the misalignment-induced astigmatism (Z5/Z6) of the NST and its parent telescope with the same aperture size are shown in Fig. 4. The specific misalignment parameters used here are XDE_{SM} = 0.05mm, YDE_{SM} = –0.08mm, ADE_{SM} = –0.005°, and BDE_{SM} = –0.004°. The length of the line in Fig. 4 represents the magnitude of the

Optics EXPRESS

astigmatism, and the direction of the line represents the direction of the astigmatism. We can see that in misaligned NST telescope, the dominant astigmatism component is field-constant and no node lies in the field of view. However, in its on-axis parent system, the misalignment-induced astigmatism is bi-nodal (in the presence of the specified misalignment parameters the two nodes are located very close to each other).

This fact can indicate that the effects of lateral misalignments and astigmatic figure error on the primary mirror couple tightly with each together in off-axis two-mirror telescopes, for both of them will contribute a large field-constant component to the astigmatic aberration field. In on-axis telescopes, the presence of on-axis astigmatism can mean an astigmatism figure error. For off-axis systems, this is not the case. Therefore, in the presence of on-axis astigmatism in off-axis systems, we should carefully analyze the causes.

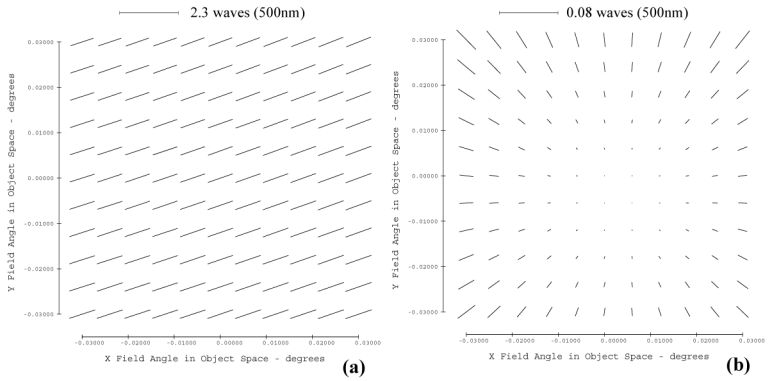

Fig. 4. FFDs for astigmatism (Z5/Z6) in the NST (a) and its parent on-axis telescope with the same aperture size (b) in the presence of the same lateral misalignments. We can see that in the misaligned NST telescope, the dominant astigmatism component is field-constant and no node lies in the field of view. However, in its on-axis parent system, the misalignment-induced astigmatism is bi-nodal (the locations of the two nodes are very close to each other in (b) in the presence of the specified misalignment parameters).

Besides, it can also be recognized from Eq. (33) that the magnitude of the field-constant astigmatism component induced by misalignments is positively associated with the magnitude of the pupil decentration vector, $\left|\vec{s}\right|$. Therefore, decreasing the value of this parameter can make the off-axis systems less sensitive to lateral misalignments. From this perspective, in the optical design off off-axis systems, we should reduce the magnitude of pupil decentration, under the premise that we can achieve an unobscured configuration.

We also point out that the magnitude of $\vec{A}_{131}^{(P)}$, $\left|\vec{A}_{131}^{(P)}\right|$, is not always larger than the magnitude of $\vec{A}_{222}^{(P)}$, $\left|\vec{A}_{222}^{(P)}\right|$. There can be coma-free pivot points in the on-axis parent telescope, about which a rotation of the particular surface leaves the coma aberration field unchanged. This means that coma can remain zero in the field of view in the presence of lateral misalignments. However, we will not further investigate this special situation. We only consider the most general cases.

For the off-axis TMA telescopes, apart from the spherical aberration, the astigmatism and coma are also corrected, i.e., $W_{222}=0$, $W_{131}=0$. For this case, we can infer from Eqs. (33)-(35) that the astigmatism in misaligned off-axis TMA telescopes can be seen as a combination of a small field-linear component and a relatively large field-constant one. Similarly, in general no node lies in the field of view.

Optics EXPRESS

Then we continue to conduct some quantitative discussion on the astigmatic aberration field. On the one hand, we use the ray tracing data to demonstrate the correctness of the analytic expressions presented in this paper. On the other hand, we explicate the discrepancies between the 3rd-order model and the 5th-order model as well as those between the 5th-order model and the ray tracing data. In the presence of the misalignments specified above, the Fringe Zernike coefficients for astigmatism (C_5/C_6) at three field points ((0,0), (0.03°,0.03°), (0.03°,-0.03°)) obtained directly from the optical simulation software and those calculated using the 3rd-order and 5th-order model are presented in Table 2.

Table 2. Verification for the Astigmatism Aberration Field in the Misaligned NST

	(0,0)		(0.03°,0.03°)		(0.03°,-0.03°)	
	C_5	C_6	C_5	C_6	C_5	C_6
Ray Tracing	0.7952	0.6439	0.7430	0.7199	0.8431	0.6684
3rd-order Model	1.0018	0.7209	0.9476	0.7968	1.0485	0.7460
5th-order Model	0.7684	0.6388	0.7155	0.7150	0.8166	0.6637

We can see from Table 2 that the 3rd-order model can still roughly represent the general trends of the astigmatism aberration field in misaligned off-axis two-mirror telescopes. Therefore, we can use the 3rd-order model to qualitatively discuss the astigmatic aberration field characteristics. On the other hand, however, we can also recognize that the 3rd-order model is not accurate enough. Apparently this is because it does not include those aberration contributions arising from the aberrations of the parent on-axis system with higher-order pupil dependence.

We here first explicate the discrepancies between 3rd-order model and 5th-order model. As mentioned in the previous part of this section, while those 5th-order aberration coefficients we considered in this paper (W_{060}, $W_{151,SM}^{(sph)}$ and $W_{151,SM}^{(asph)}$) are still very small, their effects can be greatly magnified through pupil coordinate transformation. Take the net astigmatic aberration contribution arising from the 5th-order aperture coma of the misaligned on-axis parent system as an example,

$$\left|\Delta W_{AST,51}^{(U)}\right| = \left|2\left(\vec{s}\cdot\vec{s}\right)\vec{s}\vec{C}_{51} + 2\left(\vec{s}\cdot\vec{C}_{51}\right)\vec{s}^{2}\right| \le 4\left|\vec{s}\right|^{3}\left|\vec{C}_{51}\right|, \tag{37}$$

where $\left|\Delta W_{AST,51}^{(U)}\right|$ represents the magnitude of the net astigmatic aberration contribution arising from the 5th-order aperture coma of the misaligned on-axis parent system through pupil coordinate transformation, and the condition of the inequality taking mark of equality is that the vector $\vec{C}_{51}$ has the same direction with $\vec{s}$ (For two-mirror astronomical telescopes, $W_{151}=0$, thus the specific expression of $\vec{C}_{51}$ is $\vec{C}_{51}=-\vec{A}_{151}^{(P)}$, with $\vec{A}_{151}^{(P)}=\sum_j W_{151j}\vec{\sigma}_j$). We can see from Eq. (37) that at most the magnitude of $\vec{C}_{51}$ can be magnified $4\left|\vec{s}\right|^3$ times when it is transformed into astigmatism through pupil coordinate transformation. Note that for large astronomical telescopes, the unobscured configuration is mainly achieved by pupil decenter (not field bias). In general, we can have $\left|\vec{s}\right|>2$ ($\left|\vec{s}\right|$ represents the ratio of the magnitude of pupil decenter to the half pupil size). Take the NST for example, $\left|\vec{s}\right|=2.3$, thus $4\left|\vec{s}\right|^3\approx 50$. This means that at most the magnitude of $\vec{C}_{51}$ can be magnified 50 times when it is transformed into astigmatism through pupil coordinate transformation. The case is similar to

Optics EXPRESS

the astigmatism aberration contribution arising from the 5th-order spherical aberration of the on-axis parent system, which can be expressed as

$$\left|\Delta W_{AST,60}^{(U)}\right| = \left|6W_{060}\left(\vec{s}\cdot\vec{s}\right)\vec{s}^{2}\right| = 6\left|\vec{s}\right|^{4}\left|W_{060}\right|. \tag{38}$$

For the NST, $6\left|\vec{s}\right|^{4} \approx 170$. This means the magnitude of astigmatism aberration contribution arising from the 5th-order spherical aberration of the on-axis parent system through pupil coordinate transformation is about 170 times larger than the magnitude of the 5th-order spherical aberration, W_{060}. The 3rd-order model does not include those aberration contributions arising from the 5th-order aberrations of on-axis parent system through pupil coordinate transformation, thus it is less accurate than the 5th-order model.

Then we continue to explicate the discrepancies between the results of 5th-order model and ray tracing data. We should note that the magnification effect of pupil coordinate transformation is positively associated with the order of pupil dependence of those aberrations in the on-axis parent system. While those aberration coefficients higher than 5th-order are far smaller (such as W_{080}, $W_{171,SM}^{(sph)}$ and $W_{171,SM}^{(asph)}$), the magnification effect of pupil coordinate transformation can also be larger. Therefore, they can also contribute some aberration contributions through pupil coordinate transformation. This is why there still exist some discrepancies between the 5th-order model and ray tracing data. It can be inferred that if those aberration coefficients higher than 5th-order are further considered in the derivation of the aberration expressions in misaligned off-axis systems, the discrepancies between our analytic expressions and the ray tracing data can further be reduced.

4. The inherent relationships between the astigmatic and coma aberration fields in off-axis two-mirror telescopes with lateral misalignments

In this section we further present some more in-depth discussions on the astigmatic and coma aberration fields in off-axis two-mirror telescopes with lateral misalignments. We first use the 3rd-order model to qualitatively discuss the inherent relationships between the magnitude and orientation of the astigmatic and coma aberration fields in off-axis telescopes with lateral misalignments. This knowledge can indicate that the primary mirror astigmatic figure error can be compensated with the intentionally introduced misalignments of the system. Then the 5th-order model are further used to present some quantitatively discussions concerning how to determine the specific misalignment parameters used to compensate for the effects of primary mirror astigmatic figure error as well as how to separate the effects of the primary mirror astigmatic figure error and secondary mirror lateral misalignments.

The inherent relationship between the magnitude of the misalignment-induced astigmatism and coma aberration fields in off-axis two-mirror telescopes

As discussed in the previous section, for a small field of view, the magnitude of the field-quadratic astigmatism component, W_{222}, and the field-linear astigmatism term, $\vec{A}_{222}^{(P)}$, are usually much smaller than the magnitude of the field-constant term, $\vec{A}_{131}^{(P)}\vec{s}$. Besides, the field-quadratic and field-linear components mainly affect the marginal field of view. They have little influence on the regions near the field center. Therefore, to help seize the principle points and make our discussion simpler and more direct, we here first neglect the field-quadratic and the field-linear astigmatism components. With similar reasons, we here also neglect the field-linear coma component. Under these premises, the astigmatism and coma aberration fields in the off-axis two-mirror telescopes with lateral misalignments can be given by

Optics EXPRESS

$$W_{AST}^{(U)} = -\vec{A}_{131}^{(P)}\vec{s}\cdot\vec{\rho}^{2},$$
$$W_{Coma}^{(U)} = -\vec{A}_{131}^{(P)}\cdot\vec{\rho}\left(\vec{\rho}\cdot\vec{\rho}\right). \tag{39}$$

On the other hand, in the optical alignment and testing process, aberrations are usually quantified based on the values of its Fringe Zernike coefficients. The astigmatism and coma aberration can also be expressed as

$$W_{AST}^{(U)} = \begin{bmatrix} C_5 \\ C_6 \end{bmatrix}\cdot\begin{bmatrix} \rho^2\cos(2\phi) \\ \rho^2\sin(2\phi) \end{bmatrix} = \vec{C}_{5/6}\cdot\vec{\rho}^{2},$$
$$W_{Coma}^{(U)} = \begin{bmatrix} C_7 \\ C_8 \end{bmatrix}\cdot\begin{bmatrix} (3\rho^3-2\rho)\cos(\phi) \\ (3\rho^3-2\rho)\sin(\phi) \end{bmatrix} = 3\vec{C}_{7/8}\cdot\vec{\rho}\left(\vec{\rho}\cdot\vec{\rho}\right)-2\vec{C}_{7/8}\cdot\vec{\rho}. \tag{40}$$

where $\vec{C}_{5/6} \equiv \begin{bmatrix} C_5 \\ C_6 \end{bmatrix}$, $\vec{C}_{7/8} \equiv \begin{bmatrix} C_7 \\ C_8 \end{bmatrix}$, and C_i is the *i*-th Fringe Zernike coefficient for a certain field point. Comparing Eq. (39) with Eq. (40) and neglecting the tilt term in Eq. (40) we can find that

$$\vec{C}_{5/6} = 3\vec{C}_{7/8}\vec{s}, \tag{41}$$

which clearly shows there exists inherent relationships between the magnitude and orientation of astigmatism and coma aberration fields in off-axis two-mirror telescopes with lateral misalignments. Here we first concentrate on the relationship between the magnitudes of them. Utilizing Eq. (41), we can obtain

$$\left|\vec{C}_{5/6}\right| = 3\left|\vec{s}\right|\cdot\left|\vec{C}_{7/8}\right|, \tag{42}$$

where $\left|\vec{C}_{5/6}\right| \equiv \sqrt{C_5^2+C_6^2}$, representing the magnitude of astigmatism, $\left|\vec{C}_{7/8}\right| \equiv \sqrt{C_7^2+C_8^2}$, representing the magnitude of coma, and $\left|\vec{s}\right|$ is the magnitude of the pupil decentration vector, which represents the ratio of the pupil displacement to the half pupil size. It can be seen from Eq. (42) that the magnitude of astigmatism is about $3\left|\vec{s}\right|$ times of the magnitude of coma in off-axis two-mirror telescopes in the presence of lateral misalignments. From this sense, we can consider that the astigmatism is much more detrimental to the imaging performance than coma in misaligned off-axis telescopes.

To demonstrate the statements presented above, we first introduce two sets of lateral misalignments into the NST telescope in the optical simulation software Code V®. Note that for this off-axis telescope, $\left|\vec{s}\right| = 2.3$ ($3\left|\vec{s}\right| \approx 7$). With each set of lateral misalignments, we can obtain a set of astigmatism and coma aberration fields. The two sets of astigmatism and coma aberration fields are shown in Fig. 5(a) and Fig. 5(b), respectively. The specific misalignment parameters used in Fig. 5(a) are XDE_{SM} = 0.08mm, YDE_{SM} = –0.005mm, ADE_{SM} = –0.002°, and BDE_{SM} = 0.007°. The specific misalignment parameters used in Fig. 5(b) are XDE_{SM} = –0.08mm, YDE_{SM} = –0.09mm, ADE_{SM} = 0.001°, and BDE_{SM} = –0.004°.

It can be seen from the scale labeled in Fig. 5 that Eq. (42) can roughly represent the inherent relationship between the magnitude of astigmatism and coma aberration fields induced by lateral misalignments for off-axis two-mirror telescopes. Besides, we also simulated a lot of other lateral misalignment perturbations. We find that on average the ratio

Optics EXPRESS

of the magnitude of astigmatism to coma is actually a little larger than $3\left|\vec{s}\right|$. One of the main reasons that results in this deviation is that we do not consider the effects of the high-order aberrations of the on-axis parent telescope in the derivation of Eqs. (41)-(42). However, we still consider that Eq. (42) can roughly represent the inherent relationship between the magnitude of astigmatism and coma in off-axis two-mirror telescopes with lateral misalignments using a very concise and intuitive expression.

The inherent relationship between the orientation of the astigmatism and coma aberration fields induced by lateral misalignments in off-axis two-mirror telescopes

Here we continue to discuss the inherent relationship between the orientation of the astigmatism and coma aberration fields induced by lateral misalignments for off-axis two-mirror telescopes. Referring to Eq. (38), we can write

$$\xi\left(\vec{C}_{5/6}\right)=\xi\left(\vec{s}\right)+\xi\left(\vec{C}_{7/8}\right), \tag{43}$$

where $\xi\left(\vec{A}\right)$ represents the azimuthal angle of the vector $\vec{A}$, as illustrated in Fig. 6. Here the x-axis is used as the reference axis and the azimuthal angle of a vector is measured counter-clockwise from it. Under this premise, the correspondence between the azimuthal angle and the two components of a vector can be given by

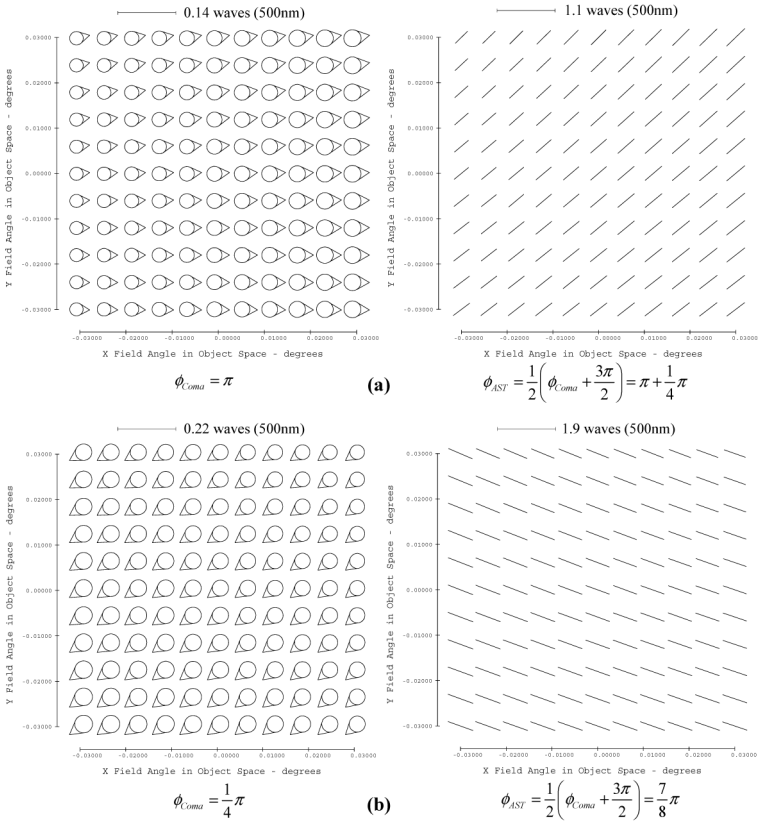

Fig. 5. FFDs used to show the inherent relationships between the magnitude and orientation of coma (Z7/Z8) and astigmatism (Z5/Z6) in the misaligned NST. We can see that these relationships can roughly be represented by Eq. (42) and Eq. (46), respectively. Here (a) and (b) are obtained in the presence of two different sets of lateral misalignments specified before.

Optics EXPRESS

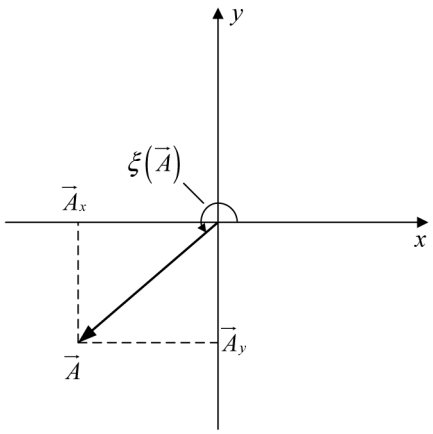

Fig. 6. Schematic representation for the azimuthal angle of a vector.

$$\xi(\vec{A})=\begin{cases}\tan^{-1}\left(\vec{A}_y/\vec{A}_x\right) & \vec{A}_x>0,\vec{A}_y\geq 0,\\ \tan^{-1}\left(\vec{A}_y/\vec{A}_x\right)+\pi & \vec{A}_x<0,\\ \tan^{-1}\left(\vec{A}_y/\vec{A}_x\right)+2\pi & \vec{A}_x>0,\vec{A}_y<0,\\ \pi/2 & \vec{A}_x=0,\vec{A}_y>0,\\ 3\pi/2 & \vec{A}_x=0,\vec{A}_y<0,\\ \text{undefined} & \vec{A}_x=0,\vec{A}_y=0.\end{cases} \tag{44}$$

Referring to Eq. (40) and references [20,22], we can link the orientation of astigmatism and coma (represented by ϕ_{AST} and ϕ_{Coma}, respectively) to the azimuthal angle of the two vectors, $\vec{C}_{5/6}$ and $\vec{C}_{7/8}$,

$$\begin{aligned}2\phi_{AST}&=\xi\left(\vec{C}_{5/6}\right),\\ \phi_{Coma}&=\xi\left(\vec{C}_{7/8}\right).\end{aligned} \tag{45}$$

Substituting Eq. (45) into Eq. (43), we have

$$2\phi_{AST}=\phi_{Coma}+\xi\left(\vec{s}\right), \tag{46}$$

which can clearly show the inherent relationship between the orientation of astigmatism and coma in off-axis telescopes with lateral misalignments.

For the NST simulated in this paper, $\vec{s}=[0,-2.3]^T$. According to Eq. (44), we can obtain that $\xi\left(\vec{s}\right)=3\pi/2$. In this case, we can see from Fig. 5 that Eq. (46) can roughly represent the inherent relationship between the orientation of astigmatism and coma aberration fields induced by lateral misalignments. Note that the orientation of astigmatism is in $[0,\pi)$ while the orientation of coma is in $[0,2\pi)$. Therefore, while in Fig. 5(a) we obtain that the orientation of astigmatism is $5\pi/4$ with Eq. (46), actually it is equivalent to $\pi/4$.

These inherent relationships between the coma and astigmatic aberration fields can also roughly apply to the case of off-axis TMA telescopes. The underlying cause that results in these inherent relationships is that the both the major components of the astigmatism and

Optics EXPRESS

coma in the off-axis telescopes with lateral misalignments are generated by the misalignment-induced coma aberration of the on-axis parent telescope through pupil coordinate transformation.

Note that these inherent relationships between the astigmatism and coma aberration fields are unique for the effects of lateral misalignments in off-axis telescopes. They can be used to roughly separate the effects of lateral misalignments and astigmatism figure error. This is because the presence of certain amount of astigmatism figure error can break the relationships between the astigmatism and coma aberration fields induced by lateral misalignments. By analyzing the deviation we can estimate the magnitude and orientation of the astigmatic figure error. In the last part of this section, we will further present a quantitative discussion on how to quantitatively separate the effects of primary mirror astigmatic figure error and lateral misalignments for off-axis two-mirror telescopes based on the astigmatic and coma aberration fields.

Compensation for primary mirror astigmatic figure error using lateral misalignments for off-axis two-mirror telescopes

After discussing the specific misalignment-induced astigmatic and coma aberration field characteristics and revealing their inherent relationships, here we show that this knowledge can lead to some valuable insights into the active compensation and alignment strategies for active optics systems in off-axis systems.

As primary mirrors get larger in diameter and relatively thinner, it is very common for them to have an astigmatic figure error, which can be induced by manufacturing error and thermal or elevation changes. In this case, a field-constant astigmatism will be introduced to the system, as the primary mirror usually serves as the aperture stop. Active optics systems with the ability of active correction for the astigmatic figure error are usually needed for on-axis large astronomical telescopes because the field-constant astigmatism can hardly be compensated by intentionally introducing misalignments to the system.

However, for off-axis telescopes with offset pupil, this is not the case. As presented in the previous parts of this paper, a large field-constant astigmatism can be introduced into the system by intentionally misaligning the system, accompanied with a field-linear astigmatism and a field-constant coma, the magnitude of which are relatively small compared to the magnitude of the field-constant astigmatism.

Then we begin to discuss how to quantitatively determine the lateral misalignments for compensating the effect of primary mirror astigmatic figure error for off-axis two-mirror telescopes. According to the 5th-order model, the process of compensating for the effects of primary mirror astigmatic figure error using lateral misalignments can be expressed as

$$-\vec{A}_{131}^{(P)}\vec{s}+2W_{040}\vec{s}^{2}-2\left(\vec{s}\cdot\vec{s}\right)\vec{s}\vec{A}_{151}^{(P)}-2\vec{s}^{2}\left(\vec{s}\cdot\vec{A}_{151}^{(P)}\right)+6W_{060}\left(\vec{s}\cdot\vec{s}\right)\vec{s}^{2}+\vec{C}_{22}^{(F)}=\vec{0}, \quad (47)$$

where $\vec{C}_{22}^{(F)}$ is the vector which represents the magnitude and orientation of the field-constant astigmatism induced by primary mirror astigmatic figure error.

On the other hand, the field-linear astigmatism can also be controlled, which can be expressed as

$$\vec{A}_{222}^{(P)}=\vec{0}, \quad (48)$$

which indicates that no field-linear astigmatism is induced when compensating for the effects of primary mirror astigmatic figure error by intentionally introducing lateral misalignments into the system. Equations (47)-(48) can be used to compute the intentionally introduced misalignment parameters.

In effect, for off-axis two-mirror telescopes with a typically small field of view, we can neglect the field-linear astigmatism induced by intentionally introduced misalignments. On

Optics EXPRESS

the other hand, we can put some constraints on the misalignment parameters used to compensate for the effects of primary mirror astigmatic figure error. For example, we can only use the decenter parameters of the secondary mirror to do this work while the tip-tilts stay unchanged, for in practice the tip-tilt parameters are hard to be precisely controlled. In this case, Eq. (47) is enough to compute the decenter parameters used to compensate for the effects of primary mirror astigmatic figure error. We should also point out that for those off-axis systems with a larger field of view, such as the off-axis TMA telescopes, the field-linear astigmatism should also be controlled. For the case of off-axis TMA telescopes, we can also put some constraints on the misalignment parameters used to compensate for the effects of primary mirror astigmatic figure error. For example, we can only use the misalignments of the secondary mirror to do this work, while the position of the tertiary mirror stay fixed.

To demonstrate the statements presented above, we introduce some amount of astigmatism to the primary mirror of the NST in the simulation software. In this case, the coma and astigmatic aberration fields are presented in Fig. 7(a). We can see that a field-constant astigmatism is induced, while the coma aberration is in the nominal state. Then we intentionally introduce some amount of lateral misalignments to compensate for it using Eq. (47), the results are shown in Fig. 7(b). It can be seen that the field-constant astigmatism has been compensated, leaving a relatively small amount of misalignment-induced coma.

The specific primary mirror figure error parameters and the intentionally introduced lateral misalignment parameters used in Fig. 7 are also presented here. The Zernike coefficients for the field-constant astigmatic aberration induced by primary astigmatic figure error are $C_5 = -0.37\lambda$, $C_6 = 0.44\lambda$ ($\lambda = 500$nm), as shown in Fig. 7(a). Here only decenter parameters are used to compensate for the effects of primary mirror astigmatic figure error. Using Eq. (47) and the relationships between misalignments and the shifted aberration field center for each individual surface [25], we can obtain the intentionally introduced decenter parameters are $XDE_{SM} = -0.048$mm, $YDE_{SM} = -0.056$mm.

This part shows that for off-axis telescopes, the effect of primary mirror astigmatic figure error can be compensated using lateral misalignments to some extent. This result can eliminate the necessity of the actuators used to actively control the figure of the primary mirror in off-axis telescopes. However, we should point out that in general it is better to separate the effects of misalignments and figure errors and correct them respectively, because this can give us an independent control over each individual component. On the other hand, this result may mean a lot to the space telescopes, for the elimination of the need for actuators can save space and reduce the cost, facilitate the design of mechanical structure and thermal control, reduce the uncertainty of the system and increase its service life.

Besides, we can also recognize that the compensation capacity of lateral misalignments for the effect of primary mirror astigmatic figure error is also positively associated with the magnitude of the pupil decentration vector, $|\vec{s}|$. For a certain amount of primary mirror astigmatic figure error, a larger $|\vec{s}|$ can mean that a smaller field-constant coma will be introduced due to intentionally misaligning the system. On the other hand, however, as mentioned above, increasing $|\vec{s}|$ can make the off-axis system more sensitive to misalignments.

Optics EXPRESS

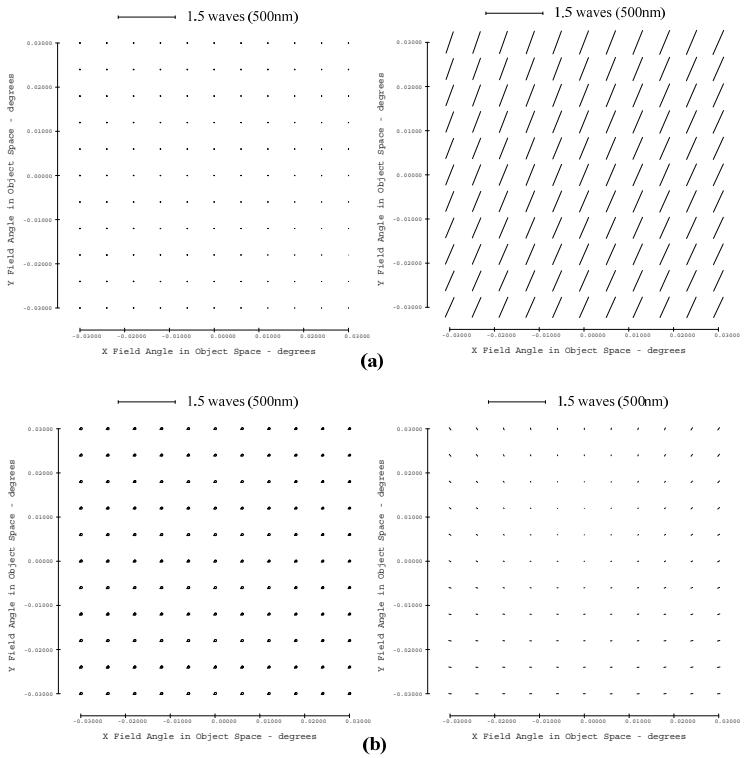

Fig. 7. FFDs used to show the compensation for the field-constant astigmatism in NST due to primary mirror astigmatic figure error by intentionally introducing lateral misalignments to the off-axis system. (a) and (b) are the coma (Z7/Z8) and astigmatism aberration fields (Z5/Z6) before and after intentionally misaligning the system. It can be seen that the field-constant astigmatism has been well compensated, leaving a relatively small amount of misalignment-induced coma.

Separation of the effects of primary astigmatic figure error and secondary misalignments for off-axis two-mirror telescopes

In the previous part of this section, we present a quantitative discussion for compensating for the effects of primary mirror astigmatic figure error using lateral misalignments of the secondary mirror. Here we continue to present a quantitative investigation for the opposite problem, i.e., separating the effects of primary mirror astigmatic figure error and secondary mirror misalignments. This problem has been discussed in detail in [23] for on-axis two-mirror telescopes. Here we will show how to extend that work to include off-axis two-mirror telescopes based on the astigmatic and coma aberration fields.

We can see from Table 1 and Table 2 that even the 5th-order model cannot express the total astigmatic and coma aberration fields to a very high accuracy. This means that it is unsuitable to directly use the total astigmatic and coma aberration fields to determine the misalignment and figure error parameters. In fact, we can only concern the changes in Fringe Zernike coefficients induced by misalignments for each field point and analytically express these changes according to the 5th-order model. In other words, we focus on the net aberration contribution induced by misalignments, not on the total aberration fields in the presence of misalignments. By doing this we can eliminate the impact of those higher-order (higher than 5th-order) aberrations of the on-axis parent system which are not affected by misalignments (such as W_{080}) on the computation accuracy of our method.

Optics EXPRESS

The net astigmatic aberration contribution due to misalignments and astigmatic figure error can be expressed as

$$\Delta W_{AST}^{(U)} = -\vec{A}_{222}^{(P)}\vec{H} + \frac{1}{2}\vec{B}_{222}^{2}, \tag{49}$$

where

$$\frac{1}{2}\vec{B}_{222}^{2} = \frac{1}{2}\vec{B}_{222}^{2(P)} - \vec{A}_{131}^{(P)}\vec{s} - 2\left(\vec{s}\cdot\vec{s}\right)\vec{s}\vec{A}_{151}^{(P)} - 2\vec{s}^{2}\left(\vec{s}\cdot\vec{A}_{151}^{(P)}\right) + \vec{C}_{22}^{(F)}. \tag{50}$$

As mentioned above, the $\vec{C}_{22}^{(F)}$ represents the astigmatism induced by primary mirror astigmatism figure error, which is directly related to the Fringe Zernike coefficients used to represent the astigmatic figure error. Using wavefront measurements at a minimum of two field points, we can determine $\vec{A}_{222}^{(P)}$ and $\vec{B}_{222}^{2}$.

The net coma aberration contribution induced by lateral misalignments can be expressed as

$$\Delta W_{131}^{(U)} = -\vec{A}_{131}, \tag{51}$$

where

$$\vec{A}_{131} = \vec{A}_{131}^{(P)} + 4\left(\vec{s}\cdot\vec{s}\right)\vec{A}_{151}^{(P)} + 4\left(\vec{s}\cdot\vec{A}_{151}^{(P)}\right)\vec{s} + \vec{s}^{2}\vec{A}_{151}^{(P)*}. \tag{52}$$

Using wavefront measurements at a minimum of one field point, we can determine $\vec{A}_{131}$.

Since $\vec{A}_{222}^{(P)}$ and $\vec{A}_{131}$ have been determined, we can further determine the field center displacement vectors associated with the spherical base curve and the aspheric departure from the secondary mirror, $\vec{\sigma}_{SM}^{(sph)}$ and $\vec{\sigma}_{SM}^{(asph)}$. Then on the one hand, these two vectors can be directly used to calculate the misalignments of the secondary mirror. On the other hand, since $\vec{B}_{222}^{2}$ and the two field center displacement vectors are known, using Eq. (50), $\vec{C}_{22}^{(F)}$ can be determined.

To demonstrate the computation accuracy of the analytic method presented in this paper, we will perform Monte Carlo computation simulations. Four different cases with different perturbation value ranges will be considered. The specific ranges for different perturbation parameters in each case are presented in Table 3, where *XDE* and *YDE* are in mm, *ADE* and *BDE* are in degree, and the Fringe Zernike coefficients for primary mirror astigmatic figure error, ${}_{F}C_{5}^{(PM)}$, ${}_{F}C_{6}^{(PM)}$, are in λ (λ = 500nm). Then we will use wavefront measurements at three field points ((0,0), (0.03°,0.03°), (0.03°,-0.03°)) to calculate them.

Table 3. Four Different Cases Considered in the Monte Carlo Simulations

	XDE_{SM}, YDE_{SM}	ADE_{SM}, BDE_{SM}	${}_{F}C_{5}^{(PM)}$, ${}_{F}C_{6}^{(PM)}$
Case 1	[-0.1,0.1]	[-0.01,0.01]	[-0.2,0.2]
Case 2	[-0.05,0.05]	[-0.005,0.005]	[-0.1,0.1]
Case 3	[-0.01,0.01]	[-0.001,0.001]	[-0.02,0.02]
Case 4	[-0.1,0.1]	[-0.01,0.01]	[-0.02,0.02]

For each case, 200 perturbation states will be randomly generated following a uniform distribution and introduced into the optical simulation software. The computation accuracy of the presented method is evaluated by the root mean square deviation (RMSD) between the introduced and computed values for each individual perturbation parameter, which is

Optics EXPRESS

expressed as $RMSD_i = \sqrt{\frac{1}{200}\sum_{n=1}^{200}\left[x_i(n) - X_i(n)\right]^2}$, where $X_i(n)$ and $x_i(n)$ represent the introduced and computed set of values for the i^{th} perturbation parameter, respectively. The computation results for different cases are presented in Table 4.

Table 4. Root Mean Square Deviations between the Introduced and Computed Values

	XDE_{SM}	YDE_{SM}	ADE_{SM}	BDE_{SM}	${}_F C_5^{(PM)}$	${}_F C_6^{(PM)}$
Case 1	1.42×10^{-3}	1.02×10^{-2}	2.21×10^{-4}	5.25×10^{-5}	2.95×10^{-2}	3.61×10^{-4}
Case 2	7.03×10^{-4}	4.94×10^{-3}	1.06×10^{-4}	2.69×10^{-5}	1.42×10^{-2}	1.54×10^{-4}
Case 3	1.52×10^{-4}	1.05×10^{-3}	2.20×10^{-5}	5.48×10^{-6}	2.91×10^{-3}	3.17×10^{-5}
Case 4	2.52×10^{-4}	1.12×10^{-2}	2.33×10^{-4}	4.62×10^{-5}	3.15×10^{-2}	3.41×10^{-4}

It can be seen that we can quantitatively separate the effects of misalignments and primary mirror astigmatism figure error for off-axis two-mirror telescopes. Besides, we can also draw several important results from Table 4:

(1) The computation accuracy for each perturbation parameter is associated with the direction of it (or the coordinate plane it lie in). We can see that those misalignment parameters in the symmetry plane (y-z plane) are computed with less accuracy, while those in x-z plane are computed more accurately. As mentioned in Section 2, the sensitivity of off-axis systems to misalignments is associated with the directions of the misalignments and one of the reasons is that the lower-order aberrations of the off-axis systems include some contributions with the factor of $\left(\vec{s}\cdot\vec{C}_{lm}\right)$. If $\vec{C}_{lm}$ is located in the x-z plane, $\vec{s}\cdot\vec{C}_{lm} = 0$. This indicates that in the x-z plane some aberration contributions arising from those higher-order aberrations of the on-axis system not included in our 5th-order model are actually equivalent to zero. Therefore the 5th-order model is more accurate in x-z plane than in y-z plane. Referring to Eq. (50) we also can infer that ${}_F C_6^{(PM)}$ is computed more accurately than ${}_F C_5^{(PM)}$.

(2) We can see from the computation results for Case 1~Case 3 that the absolute computation accuracy of each parameter has a strong correlation with the magnitude of misalignments. Specifically, a small perturbation range can mean a small deviation between the introduced value and the computed value. The main reason for this is that when the magnitude of the misalignments is small, the aberration contributions arising from those higher-order aberrations of the on-axis system not included in our 5th-order model is also small, i.e., our 5th-order model is more accurate.

(3) Comparing Case 1 with Case 4 we also find that when the magnitude of misalignments is large while the magnitude of astigmatic figure error is small, the astigmatic figure error cannot be computed accurately. Therefore, in practice, we can correct the misalignments first, and when the misalignments are nearly corrected, we begin to correct the astigmatic figure error (here we do not consider compensating for the effects of astigmatic figure error using misalignments).

For the case of off-axis TMA telescopes, it is more difficult to separate the effects of misalignments and primary mirror astigmatic figure error. One the one hand, TMA telescopes have more degrees of freedom, thus the astigmatic and coma aberration fields are not enough for solving them. On the other hand, the 5th-order model for expressing each aberration field

Optics EXPRESS

in misaligned off-axis TMA telescopes is more complicated than in off-axis two-mirror telescopes. TMA telescopes have a relatively larger field of view. Therefore, some 5th-order aberration coefficients that can be neglected for off-axis two-mirror telescopes should be considered for off-axis TMA telescopes. However, we can still use the similar method to achieve this goal. We can first analytically express different kinds of aberration fields (such as astigmatism, coma and medial focal surface) in the presence of misalignments and astigmatic figure error, and then use wavefront measurements at several field points to establish equations and solve them. Besides, the boresight error (pointing error or image plane displacement), which is directly related to the misalignment parameters and can hardly be affected by figure errors, can also help us to separate these two effects.

One of the advantages of our analytic method over those numerical ones is that we need not obtain the sensitivity matrix of the wavefront to different perturbation parameters for several certain field points in advance. In practice, the suitable guide stars are not always located at those certain field points. Therefore, they usually need re-adjust the boresight to locate the suitable guide stars at those certain field points, which can definitely increase the uncertainty and inefficiency of wavefront sensing and control commissioning process. By contrast, our analytic method can use wavefront measurements at several arbitrary field points to achieve our goal.

5. Some other effects of lateral misalignments on the aberration fields of off-axis two-mirror telescopes

In this section, some other effects of lateral misalignments on the aberration fields of off-axis two-mirror telescopes will be discussed, including medial focal surface and trefoil aberration. By discussing the medial focal surface induced by lateral misalignments, we will show that for off-axis systems, the effects of lateral misalignments couple more tightly together with axial misalignments compared to on-axis systems, and the sensitivity of off-axis systems to misalignments is associated with the directions of the misalignments. A brief discussion will also be given to one of the higher-order aberrations of off-axis systems in the presence of lateral misalignments, i.e., trefoil or elliptical coma, for the completeness of this work. On the one hand, we show that in off-axis systems trefoil is more sensitive to lateral misalignments than on-axis systems. This fact indicates that the effects of lateral misalignments couple more tightly with trefoil deformations in off-axis telescopes. On the other hand, we also present a quantitative discussion for why trefoil aberration in off-axis telescopes is far more sensitive to misalignments that in on-axis ones.

Medial focal surface of off-axis two-mirror telescopes in the presence of lateral misalignments

Referring to the 3rd-order model (Eqs. (22)-(23)), the medial focal surface of off-axis telescopes in the presence of lateral misalignments can be given by

$$W_{MS}^{(U)} = C_{20}^{(U)} \cdot \left(\vec{\rho}\cdot\vec{\rho}\right) \equiv \left(C_{20} + C_{20}^{(T)}\right) \cdot \left(\vec{\rho}\cdot\vec{\rho}\right), \tag{53}$$

where we have separated the medial focal surface into two components, i.e., the one which is the same as the medial focal surface in misaligned on-axis systems,

$$C_{20} = \sum_j \left[W_{020\,j} + W_{220M\,j} \left(\vec{H} - \vec{\sigma}_j\right) \cdot \left(\vec{H} - \vec{\sigma}_j\right) \right], \tag{54}$$

and the other one which is generated by the coma and spherical aberration of the on-axis parent system through pupil coordinate transformation,

$$C_{20}^{(T)} = \sum_j \left[2W_{131\,j} \left(\vec{H} - \vec{\sigma}_j\right) \cdot \vec{s} + 4W_{040\,j} \left(\vec{s}\cdot\vec{s}\right) \right]. \tag{55}$$

Optics EXPRESS

The medial focal surface in misaligned on-axis systems has been discussed in [11], and we will not discuss it further. As discussed before, in the presence of misalignments, the magnitude of coma and spherical aberration coefficients are far smaller than the magnitude of $\vec{A}_{131}^{(P)}$, and here we neglect them. In this case, Eq. (53) can be rewritten as

$$W_{MS}^{(U)} = \left[C_{20} - 2\left(\vec{A}_{131}^{(P)} \cdot \vec{s} \right) \right] \cdot \left(\vec{\rho} \cdot \vec{\rho} \right). \tag{56}$$

It can be seen that in off-axis telescopes there is an additional field-constant focal shift compared to the medial focal surface in those on-axis telescopes in the presence of lateral misalignments, as illustrated in Fig. 8. The specific misalignment parameters used in Fig. 8 are XDE_{SM} = 0.07mm, YDE_{SM} = –0.02mm, ADE_{SM} = –0.008°, and BDE_{SM} = –0.006°. The circle in Fig. 8 represents the magnitude of defocus for a certain field point.

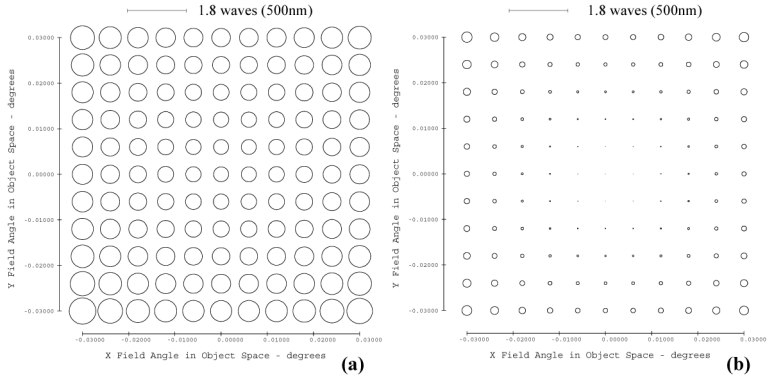

Fig. 8. FFDs for medial focal surface (Z4) in the NST (a) and its on-axis parent telescope (b) with the same lateral misalignments specified above. It can be seen that there is an additional field constant focal shift in (a) compared to the medial focal surface in (b).

Importantly, it can be inferred that for off-axis telescopes, the effects of lateral misalignments and axial misalignments couple more tightly together, for in on-axis telescopes, field-constant focal shift, is usually induced by axial misalignments. Therefore, we should carefully analyze the aberration fields of the system before we determine the causes of the field-constant focal shift that may arise in the off-axis systems.

The Fringe Zernike coefficient for the medial focal surface (C_4) obtained directly from the optical simulation software and those calculated using the 3rd-order model and the 5th-order model are presented below.

Table 5. Verification for the Medial Focal Surface in the Misaligned NST

	(0,0)	(0.03°,0.03°)	(0.03°,-0.03°)
	C_4	C_4	C_4
Ray Tracing	–0.4629	–0.7106	–0.7899
3rd-order Model	–0.5497	–0.7985	–0.8732
5th-order Model	–0.4522	–0.7010	–0.7758

We can see from Table 5 that the case for medial focal surface is similar with coma and astigmatic aberration presented in Table 1 and Table 2. On the one hand, the 3rd-order model can roughly represent the general trend of medial focal surface in misaligned off-axis two-mirror telescopes. However, it is not accurate enough. On the other hand, the 5th-order model is more accurate. However, there still exist some discrepancies between the 5th-order model and the ray tracing data. The reason for this is also similar with the case of coma and astigmatism.

Optics EXPRESS

Besides, it is also important to recognize that the magnitude of the additional field-constant focal shift in off-axis telescopes is determined by the dot product of two vectors. The direction of $\vec{s}$ is constant while the direction of $\vec{A}_{131}^{(P)}$ is dependent on the directions of misalignments. Considering that the dot product of two vectors is related to the angle between them, therefore, the magnitude of this field-constant focal shift is tightly associated with the directions of the lateral misalignment parameters. The off-axis system is plane symmetric in the nominal state, and the vector $\vec{s}$ is located in the symmetry plane. According to the vector identity of dot product, the magnitude of $\vec{A}_{131}^{(P)} \cdot \vec{s}$ is determined by the projection of $\vec{A}_{131}^{(P)}$ on $\vec{s}$. Specifically, supposing the vector $\vec{s}$ is located in the y axis direction, then the magnitude of the additional field-constant focal shift is nearly equivalent to $2\left|\vec{s}\right|\vec{A}_{131,y}^{(P)}$. In other words, no additional field-constant focal shift will be induced if the direction of $\vec{A}_{131}^{(P)}$ is perpendicular to $\vec{s}$.

We introduce a set of lateral misalignments into the NST in the optical simulation software. They are XDE_{SM} = 0.07mm, YDE_{SM} = 0mm, ADE_{SM} = 0°, and BDE_{SM} = –0.006°, i.e., the misalignments in the x-z plane are retained, while the misalignments in the y-z plane are set to zero. Therefore, the directions of the misalignments are perpendicular to the symmetry plane of the off-axis system. In this case, the medial focal surface in the misaligned NST and the nominal NST are shown in Fig. 9, respectively. We can see that in this case no field-constant focal shift is induced in the off-axis system.

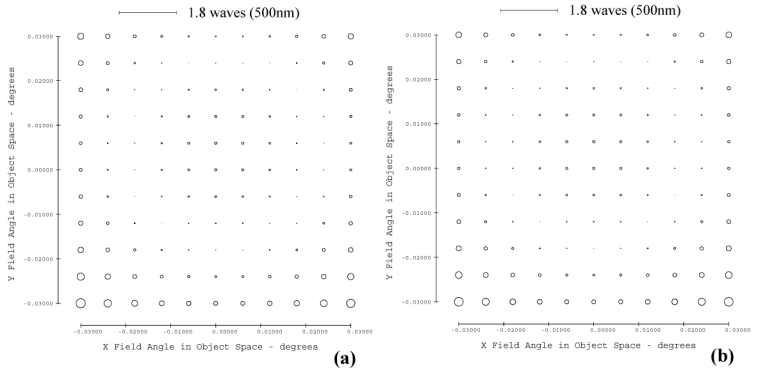

Fig. 9. FFDs for medial focal surface (Z4) in the misaligned NST (a) and the nominal NST (b) when the directions of the lateral misalignments are perpendicular to the symmetry plane. It can be seen that in this case no field-constant focal shift is induced.

Comparing Fig. 8 with Fig. 9, we can recognize that the sensitivity of off-axis systems to misalignments is associated with the directions of the lateral misalignment parameters. The underlying cause is that when the pupil is offset, the rotational symmetry of the previous on-axis system is broken, and only a plane symmetric property of the system is maintained.

Note that the magnitude of the field-constant focal shift is also positively associated with the magnitude of pupil decentration. Therefore, reducing the magnitude of pupil decentration can make the off-axis systems less likely to suffer the field-constant focal shift induced by lateral misalignments.

The Fringe Zernike coefficient for the medial focal surface (C_4) obtained directly from the optical simulation software and those calculated using the 3rd-order model and 5th-order model for the case where the misalignments are perpendicular to the symmetry plane are presented in Table 6.

Optics EXPRESS

Table 6. Verification for the Medial Focal Surface in the Misaligned NST when the Misalignments are Perpendicular to the Symmetry Plane

	(0,0)	(0.03°,0.03°)	(0.03°,-0.03°)
	C_4	C_4	C_4
Ray Tracing	0.0717	–0.1677	–0.2622
3rd-order Model	0.0795	–0.1603	–0.2531
5th-order Model	0.0695	–0.1703	–0.2632

One the one hand, we can see that the 5th-order model are still more accurate than the 3rd-order model, and there still exist some discrepancies between the 5th-order model and the ray tracing data. However, on the other hand, we can recognize that the absolute deviations between the 3 sets of data are smaller. This is because some aberration contributions arising from those higher-order aberrations of the on-axis system not included in our 3rd-order model and 5th-order model are actually equivalent to zero when the misalignments are perpendicular to the symmetry plane.

The case is similar to the off-axis TMA telescopes, i.e., a field-constant focal shift will also be induced by lateral misalignments in off-axis TMA telescopes, which is still only sensitive to those lateral misalignments in the symmetry plane of the nominal off-axis system.

Trefoil aberration field of off-axis two-mirror telescopes in the presence of lateral misalignments

Here we give a brief discussion to the trefoil aberration in off-axis telescopes with lateral misalignments. On the one hand, we show that the effects of lateral misalignments couple tightly with trefoil deformation in off-axis two-mirror telescopes. On the other hand, we quantitatively discuss the reason for this.

According to Eqs. (24-25), when the 5th-order aberrations of the on-axis parent system are considered, the trefoil aberration of misaligned off-axis systems can be given by

$$W_{Trefoil}^{(U)} = \vec{C}_{33}^{(U)} \cdot \vec{\rho}^3 \equiv \left(\vec{C}_{33} + \vec{C}_{33}^{(T)} \right) \cdot \vec{\rho}^3, \tag{57}$$

where

$$\vec{C}_{33} = \sum_j \frac{1}{4} W_{333j} \left(\vec{H} - \vec{\sigma}_j \right)^3, \tag{58}$$

representing the trefoil component which is the same as the trefoil aberration existing in misaligned on-axis systems, and

$$\vec{C}_{33}^{(T)} = \sum_j \left[\frac{1}{2} W_{242j} \left(\vec{H} - \vec{\sigma}_j \right)^2 \vec{s} + W_{151j} \left(\vec{H} - \vec{\sigma}_j \right) \vec{s}^2 + 2 W_{060j} \vec{s}^3 \right], \tag{59}$$

which represents the additional trefoil aberration contribution generated by some other aberrations of the on-axis parent system . This additional trefoil contribution resulting from pupil coordinate transformation can be far larger than the trefoil component existing in misaligned on-axis systems. The trefoil aberration in the NST telescope and its parent on-axis telescope in the presence of the same lateral misalignments are shown in Fig. 10. The specific misalignment parameters used in Fig. 10 are list as follows: XDE_{SM} = 0.08mm, YDE_{SM} = 0.06mm, ADE_{SM} = 0.004°, and BDE_{SM} = –0.006°. In Fig. 10, the length of the arrow represents the magnitude of trefoil aberration for a certain field point and the head of the arrow points to the direction of the trefoil aberration.

Optics EXPRESS

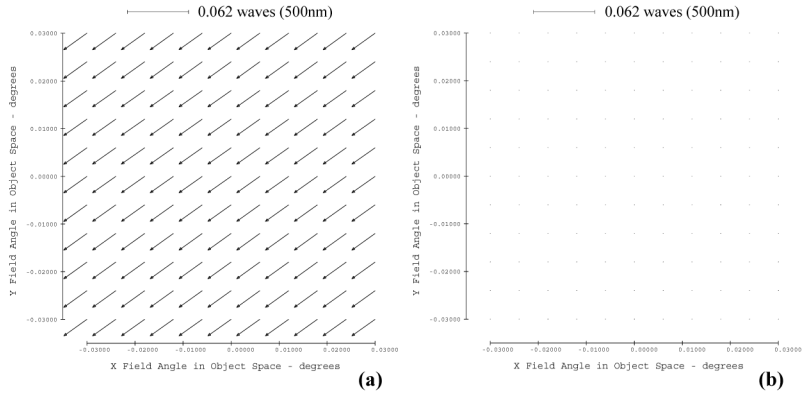

Fig. 10. FFDs for the trefoil aberration (Z10/Z11) in the NST and its parent on-axis telescope in the presence of the same lateral misalignments specified above. On the one hand, the magnitude of the trefoil in the off-axis telescope is far larger than that in its on-axis parent telescope; on the other hand, the misalignment-induced trefoil aberration is field-constant. These results indicate that in off-axis two-mirror telescopes, the effects of misalignments and trefoil deformation couple tightly with each other.

We can see that magnitude of the trefoil in the misaligned off-axis NST telescope is far larger than that in its on-axis parent telescope with the same lateral misalignments, and we also can recognize that the misalignment-induced trefoil aberration is field-constant for off-axis two-mirror telescopes. Furthermore, considering that the trefoil aberration induced by trefoil figure error is also field-constant [21, 23], we can conclude that the effects of lateral misalignments couple more tightly with trefoil deformations. Therefore, if we find some trefoil aberration in the off-axis telescopes, we should carefully analyze the causes, because for off-axis telescopes we can no longer think that the trefoil figure error is the only cause of trefoil aberration.

Then we continue to present a quantitative discussion on the reason why trefoil aberration is more sensitive to misalignments in off-axis two-mirror telescopes. For the NST telescope with the misalignment parameters specified above, the trefoil aberration (represented by the Fringe Zernike coefficients, C_{10} and C_{11}) in the three field points, i.e., (0,0), (0.03°, 0.03°), (0.03°,-0.03°) directly obtained from the simulation software and those calculated using the 5th-order model are presented in Table 7. Note that for trefoil aberration, only the 5th-order model can be used in the calculation.

Besides, for a better interpretation of the dominant cause for the trefoil aberration in misaligned off-axis two-mirror telescopes, we here further propose a simplified 5th-order model for trefoil aberration. As discussed before, for the traditional two-mirror telescopes with a small field of view, we can neglect most of the 5th-order aberration coefficients apart from W_{060}, $W_{151,SM}^{(sph)}$ and $W_{151,SM}^{(asph)}$ (the primary mirror serves as the coordinate reference so we need not consider $W_{151,PM}^{(sph)}$ and $W_{151,PM}^{(asph)}$). On the other hand, considering that the trefoil aberration arising from the 5th-order spherical aberration (W_{060}) of the on-axis parent system through pupil coordinate transformation is not affected by misalignments, we here further neglect it. Therefore, the net trefoil aberration induced by lateral misalignments for off-axis two-mirror telescopes can be expressed as

$$ {}_{M}W_{Trefoil}^{(U)} = -\vec{A}_{151}^{(P)\to 2}\vec{s}\cdot\vec{\rho}^{3}, \tag{60} $$

which is named as the "simplified 5th-order model" for trefoil aberration. Using this simplified 5th-order model we can further obtain a set of Fringe Zernike coefficients which are also presented in Table 7.

Optics EXPRESS

Table 7. Verification for the Trefoil Aberration in the Misaligned NST

	(0,0)		(0.03°,0.03°)		(0.03°,-0.03°)	
	C_{10}	C_{11}	C_{10}	C_{11}	C_{10}	C_{11}
Ray Tracing	–0.0236	–0.0169	–0.0236	–0.0169	–0.0236	–0.0169
5th-order Model	–0.0280	–0.0223	–0.0280	–0.0223	–0.0280	–0.0223
Simplified 5th-order Model	–0.0280	–0.0204	–0.0280	–0.0204	–0.0280	–0.0204

While the results of the simplified 5th-order model seem closer to the ray tracing data, however, we cannot consider that the simplified 5th-order model is more accurate than the 5th-order model. In effect, this only indicates that the net aberration contribution arising from the 5th-order spherical aberration of the on-axis system through pupil coordinate transformation has the opposite sign with the aberration contributions arising from those higher-order aberrations of the on-axis system not included in our 5th-order model.

On the other hand, while the simplified 5th-order model is not accurate enough, we can still be sure that it can roughly represent the trefoil aberration in off-axis two-mirror telescopes. Therefore, we can now explain why the trefoil aberration in the off-axis two-mirror telescopes is more sensitive to misalignments. In the on-axis two-mirror telescopes, the 5th-order aperture coma is more sensitive to misalignments than trefoil aberration. This misalignment-induced 5th-order aperture coma can be transformed into trefoil in the off-axis telescopes through pupil coordinate transformation.

For the case of off-axis TMA telescopes, it becomes harder to discuss the trefoil aberration in the presence of misalignments, for some 5th-order aberration coefficients that can be neglected for off-axis two-mirror telescopes should be considered for off-axis TMA telescopes. However, the dominant cause for the trefoil aberration in the presence of misalignments stays the same, i.e., the trefoil aberration mainly arises from the misalignment-induced 5th-order aperture coma of the on-axis system through pupil coordinate transformation.

6. Conclusion

In this paper, we investigate the aberration field characteristics of off-axis two-mirror telescopes induced by lateral misalignments. One of the focuses is placed on revealing and illustrating the differences between the misalignment-induced aberration fields of off-axis telescopes and the on-axis ones, which can also be seen as the effects of pupil decentration on the aberration fields of telescopes with lateral misalignments. We consider that an off-axis telescope with lateral misalignments is obtained by decentering the pupil of a misaligned on-axis system while the other elements of the system stay unchanged. Based on this concept, we derive the aberration function for the off-axis telescopes with lateral misalignments using the framework of nodal aberration theory and a system level pupil coordinate transformation. Then on the one hand we present a general description of the aberration fields of off-axis telescopes with lateral misalignments. On the other hand, we present some more specific aberration field characteristics induced by lateral misalignments for off-axis two-mirror telescopes, mainly including astigmatism, coma and field curvature, where the differences between the aberration fields of misaligned off-axis systems and the on-axis ones are further illustrated.

Another focus of this work is laid on providing some valuable insights and theoretical guidance for the optical design, alignment and active compensation and alignment of off-axis telescopes based on the knowledge of the aberration fields induced by lateral misalignments:

(1) We show that the both the magnitudes of the astigmatism and field-constant focal shift, which are two of the most dominant effects of lateral misalignments, are positively associated with the magnitude of pupil decenter. From this perspective, in the optical design of off-axis systems, we should reduce the magnitude of pupil

Optics EXPRESS

decenter to make off-axis systems less sensitive to misalignments under the premise that we can achieve an unobscured configuration.

(2) We show that the effects of lateral misalignments and astigmatic figure error on the primary mirror couple tightly with each together, for both of them will contribute a field-constant component to the aberration fields. In on-axis telescopes, the presence of on-axis astigmatism can mean an astigmatism figure error. For off-axis systems, this is not the case. Therefore, in the presence of on-axis astigmatism in off-axis systems, we should carefully analyze the causes.

(3) We reveal and explicate the inherent relationships between the astigmatism and coma aberration fields induced by lateral misalignments. These inherent relationships are unique for the effects of lateral misalignments. Therefore, in practice if we find a large deviation from these inherent relationships when analyzing the astigmatic and coma aberration fields for a perturbed off-axis system, we can be sure that there exist other effects, such as the primary mirror astigmatic figure error, that contribute to the net aberration fields.

(4) We also illustrate that the effects of primary mirror astigmatic figure error can be compensated by intentional misaligning the off-axis system, and increasing the magnitude of pupil decenter can increase the compensation capacity of lateral misalignments for the effects of primary mirror astigmatic figure error (while making the off-axis system more sensitive to misalignments).

(5) By discussing the effects of lateral misalignments on the medial focal surface, we show that there exists strong coupling relation between effects of lateral misalignments and axial misalignments in off-axis systems. Therefore, if we find some amount of field-constant focal shift in an off-axis telescope, we should carefully analyze the causes.

(6) Considering that this field-constant focal shift only sensitive to the lateral misalignments in the symmetry plane of the nominal off-axis system, in practice, we can impose more tight constraints on these degrees of freedom to reduce this effect.

(7) By discussing the effects of lateral misalignments on the trefoil aberration field, we show that the effects of lateral misalignments couple more tightly with trefoil deformations. Therefore, if we find some trefoil aberration in the off-axis telescopes, we should carefully analyze the causes.

The last focus of this paper is on presenting some quantitative discussions concerning the aberration fields of off-axis telescopes with lateral misalignments. The quantitative discussion not only can demonstrate the correctness and accuracy of the proposed analytic expressions for the aberration fields in misaligned off-axis systems, but also can help us to excavate the deeper reasons that result in the characteristic features of the misalignment-induced aberration fields in off-axis systems. For example, through quantitative discussion we can easily understand the main reason for why trefoil aberration in off-axis systems is more sensitive to misalignments than in on-axis systems. Therefore, on the one hand, we compare the results calculated with our 3rd-order model and 5th-order model to the real-ray tracing data. We explicitly present the reasons for why the 5th-order model is more accurate than the 3rd-order model as well as why there still exist some discrepancies between our 5th-order model and ray tracing data. On the other hand, we use the NST telescope as an example to show how to determine the specific misalignment parameters used to compensate for the effects of astigmatic figure error on the primary mirror as well as how to quantitatively separate the effects of the primary mirror astigmatic figure error and secondary mirror lateral misalignments.

Optics EXPRESS

Note that not all the unobscured off-axis telescopes can be obtained by decentering the pupil of an axisymmetric on-axis system. There can be tilted/decentered components and freeform surfaces in the nominal design of an off-axis telescope [27, 28]. It seems that this work cannot apply to them. In effect, however, in the misaligned states, their dominant aberration fields are similar to those telescopes discussed in this paper. Furthermore, while this work mainly use the off-axis two-mirror telescopes as an important example to discuss the aberration fields of off-axis telescopes, this work can be extended to other types of off-axis telescopes, such as off-axis TMA telescopes.

This work can facilitate a deep understanding of the aberration fields of off-axis telescopes induced by lateral misalignments. Besides, the effects of axial misalignments on the aberration fields of off-axis telescopes are also different from those in on-axis systems, which also require further study for better understand.

Appendix A: The derivation of the vector identity given by Eq. (2)

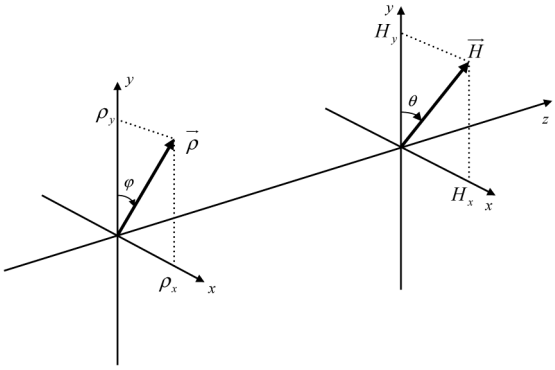

Fig. 11. Conventions for the pupil vector $\vec{\rho}$ and field vector $\vec{H}$ in nodal aberration theory.

According to the conventions of nodal aberration theory for field vector $\vec{H}$ and pupil vector $\vec{\rho}$, as illustrated in Fig. (11), we have

$$\vec{H} = H\exp(\mathrm{i}\theta),\ \vec{\rho} = \rho\exp(\mathrm{i}\varphi). \tag{61}$$

According to the vector identity of dot product, we have

$$\left(\vec{H}\cdot\vec{\rho}\right)^m = H^m\rho^m\cos^m\delta,\ \delta = \theta - \varphi. \tag{62}$$

Then using the Euler's formula,

$$\exp(\mathrm{i}\delta) = \cos\delta + \mathrm{i}\sin\delta, \tag{63}$$

we can write

$$\cos\delta = \frac{\exp(\mathrm{i}\delta)+\exp(-\mathrm{i}\delta)}{2}. \tag{64}$$

If m is an odd number,

Optics EXPRESS

$$\begin{aligned}\cos^m\delta &= \left[\frac{\exp(\mathrm{i}\delta)+\exp(-\mathrm{i}\delta)}{2}\right]^m \\ &= \frac{1}{2^m}\sum_{t=0}^{m}\binom{m}{t}\left[\exp(\mathrm{i}\delta)\right]^{m-t}\left[\exp(-\mathrm{i}\delta)\right]^t \\ &= \frac{1}{2^m}\sum_{t=0}^{\frac{m-1}{2}}\binom{m}{t}\left\{\left[\exp(\mathrm{i}\delta)\right]^{m-2t}+\left[\exp(-\mathrm{i}\delta)\right]^{m-2t}\right\} \\ &= \frac{1}{2^{m-1}}\sum_{t=0}^{\frac{m-1}{2}}\binom{m}{t}\cos\left[(m-2t)\delta\right],\end{aligned} \tag{65}$$

Therefore,

$$\begin{aligned}\left(\vec{H}\cdot\vec{\rho}\right)^m &= \frac{1}{2^{m-1}}\sum_{k=0}^{\frac{m-1}{2}}\binom{m}{t}H^m\rho^m\cos\left[(m-2t)\delta\right] \\ &= \frac{1}{2^{m-1}}\sum_{t=0}^{\frac{m-1}{2}}\binom{m}{t}H^{2t}\rho^{2t}\left\{H^{m-2t}\rho^{m-2t}\cos\left[(m-2t)\delta\right]\right\}.\end{aligned} \tag{66}$$

According to vector multiplication of nodal aberration theory, we have

$$H^{2t}=\left(\vec{H}\cdot\vec{H}\right)^t,\ \rho^{2t}=\left(\vec{\rho}\cdot\vec{\rho}\right)^t, \tag{67}$$

and

$$H^{m-2t}\rho^{m-2t}\cos\left[(m-2t)\varphi\right]=\vec{H}^{m-2t}\cdot\vec{\rho}^{m-2t}. \tag{68}$$

Substituting Eq. (67) and Eq. (68) into Eq. (66), we obtain

$$\left(\vec{H}\cdot\vec{\rho}\right)^m=\sum_{t=0}^{\frac{(m-1)}{2}}\frac{1}{2^{m-1}}\binom{m}{t}\left(\vec{H}\cdot\vec{H}\right)^t\left(\vec{\rho}\cdot\vec{\rho}\right)^t\vec{H}^{m-2t}\cdot\vec{\rho}^{m-2t}, \tag{69}$$

Similarly, if m is an even number, we can obtain

$$\left(\vec{H}\cdot\vec{\rho}\right)^m=\sum_{t=0}^{\frac{m}{2}-1}\frac{1}{2^{m-1}}\binom{m}{t}\left(\vec{H}\cdot\vec{H}\right)^t\left(\vec{\rho}\cdot\vec{\rho}\right)^t\vec{H}^{m-2t}\cdot\vec{\rho}^{m-2t}+\frac{a_m^{(m/2)}}{2}\left(\vec{H}\cdot\vec{H}\right)^{\frac{m}{2}}\left(\vec{\rho}\cdot\vec{\rho}\right)^{\frac{m}{2}}. \tag{70}$$

Appendix B: The derivation of the vector identity given by Eq. (20)

Supposing the three vectors $\vec{A}$, $\vec{B}$ and $\vec{C}$ can be expressed as

$$\vec{A}=a\exp(\mathrm{i}\alpha),\vec{B}=b\exp(\mathrm{i}\beta),\vec{C}=c\exp(\mathrm{i}\gamma), \tag{71}$$

we have

$$2\left(\vec{A}\cdot\vec{C}^p\right)\left(\vec{B}\cdot\vec{C}^q\right)=2abc^{p+q}\cos(\alpha-p\gamma)\cos(\beta-q\gamma). \tag{72}$$

Using trigonometric formulas, we can obtain

Optics EXPRESS

$$2\cos(\alpha-p\gamma)\cos(\beta-q\gamma)=\cos\left[(\alpha+\beta)-(p+q)\gamma\right]+\cos\left[(\alpha+q\gamma)-(\beta+p\gamma)\right], \quad (73)$$

Substituting Eq. (73) into Eq. (72) and referring to the vector multiplication of nodal aberration theory, Eq. (72) can be rewritten as

$$2\left(\vec{A}\cdot\vec{C}^{p}\right)\left(\vec{B}\cdot\vec{C}^{q}\right)=\vec{A}\vec{B}\cdot\vec{C}^{p+q}+\vec{A}\vec{C}^{q}\cdot\vec{B}\vec{C}^{p}, \quad (74)$$

Then using another vector identity of nodal aberration theory,

$$\vec{A}_1\vec{A}_2\cdot\vec{A}_3=\vec{A}_1\cdot\vec{A}_2^{\,*}\vec{A}_3, \quad (75)$$

where $\vec{A}_2^{\,*}$ represents the conjugate vector of $\vec{A}_2$, Eq. (74) can further be rewritten as

$$2\left(\vec{A}\cdot\vec{C}^{p}\right)\left(\vec{B}\cdot\vec{C}^{q}\right)=\begin{cases}\vec{A}\vec{B}\cdot\vec{C}^{p+q}+\left(\vec{A}\vec{B}^{*}\cdot\vec{C}^{p-q}\right)\left(\vec{C}\cdot\vec{C}\right)^{q}, & p>q,\\ \vec{A}\vec{B}\cdot\vec{C}^{p+q}+\left(\vec{A}^{*}\vec{B}\cdot\vec{C}^{q-p}\right)\left(\vec{C}\cdot\vec{C}\right)^{p}, & p<q,\\ \vec{A}\vec{B}\cdot\vec{C}^{2p}+\left(\vec{A}\cdot\vec{B}\right)\left(\vec{C}\cdot\vec{C}\right)^{p}, & p=q.\end{cases} \quad (76)$$

Appendix C: The optical prescription and layout of the NST telescope

The optical prescription and layout of the NST are presented in Table 8 and Fig. 12, respectively.

Table 8. Optical Prescription of the NST Telescope after Fold Mirrors Removed

	Radius	Conic	Thickness
M1	–7700	–1	–4150.05
M2	573.5828	–0.83087	6490.259
FP	FLAT	0.0000	

Radius and *Thickness* are in mm.

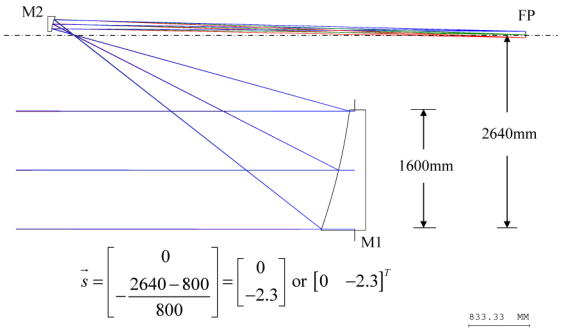

Fig. 12. Layout of the NST telescope after fold mirrors removed.

Appendix D: The 3rd-order aberration coefficients for the on-axis parent telescope of the NST

In Table 9 we list the 3rd-order aberration coefficients needed in this paper. Since we use the primary mirror as the coordinate reference, the aberration coefficients associated with the spherical base and aspheric departure of the primary mirror are not needed, so we do not list them.

Optics EXPRESS

Table 9. 3rd-order Aberration Coefficients for On-axis Parent Telescope of the NST

	W_{040}	W_{131}	W_{222}	W_{220M}
M1(sph)	\	\	\	\
M1(asph)	\	\	\	\
M2(sph)	33.2740	4.3851	0.1445	–0.1398
M2(asph)	–33.2665	4.6376	–0.1619	–0.1616
Total	0.0075	–0.0204	0.0284	–0.3003

The aberration coefficients are computed at a field angle of 0.03°, at a wavelength of 0.5 μm.

Funding

National High Technology Research and Development Program of China (Grant No. 2011AA12A103).